Direct simulation of the sedimentation of elliptic particles in Oldroyd-B fluids

By P. Y. HUANG[1], H. H. HU[2] and D. D. JOSEPH[1]

[1] Department of Aerospace Engineering and Mechanics *and* the Minnesota Supercomputer Institute, University of Minnesota, Minneapolis, MN 55455-0153, USA

[2] Department of Mechanical Engineering and Applied Mechanics, University of Pennsylvania, Philadelphia, PA 19104-6315, USA

Cross-stream migration and stable orientations of elliptic particles falling in an Oldroyd-B fluid in a channel are studied. We show that the normal component of the extra stress on a rigid body vanishes; lateral forces and torques are determined by the pressure. Inertia turns the long side of the ellipse across the stream and elasticity turns it along the stream; tilted off-centre falling is unstable. There are two critical numbers: the elasticity and Mach numbers. When the elasticity number is smaller than critical the fluid is essentially Newtonian with broadside-on falling at the centreline of the channel. For larger elasticity numbers the settling turns the long side of the particle along the stream in the channel centre for all velocities below a critical one, identified with a critical Mach number of order one. For larger Mach numbers the ellipse flips into broadside-on falling again. The critical numbers are functions of the channel blockage ratio, the particle aspect ratio and the retardation/relaxation time ratio of the fluid. Two ellipses falling near to each other, attract, line-up vertically and straighten-out with long sides vertical. Stable, off-centre tilting is found for ellipses falling in shear-thinning fluids and for cylinders with flat ends in which particles tend to align their longest diameter with gravity.

1. Introduction

Direct simulation uses the full power of computers to obtain exact solutions of initial-boundary value problems for the motion of dispersed particles, here rigid solids, in a liquid. Of course, such solutions can be no more exact than the numerical methods, but they are faithful to the underlying dynamics in which rigid bodies move under Newton's laws impelled by hydrodynamic forces arising from the solutions of the fluid equations at each nodal point in the fluid. The solutions of initial-value problems for thousands of particles in three-dimensions is not a dream for the future, but is an immediate goal towards which this paper takes one small step. Hu (1996) has already reported simulations of sedimenting and shear flows of 400 spherical particles (disks in two-dimensions) and simulations of thousands of these disks in Newtonian fluids and hundreds in viscoelastic fluids will be reported soon (see Direct simulation of particles in flowing liquids: NSF Grand Challenge Project: http//www.aem.umn.edu/Solid-Liquid_Flows/ for more information and video animations).

The solution of initial-value problems is the goal of analysis of dynamical systems leading to understanding of how systems dynamics depend on initial conditions, the nature of transients and the characterizing features of sets of permanent solutions which evolve after transients decay.

Direct two-dimensional simulations of the sedimentation of spherical particles (disks) in a vertical channel filled with an Oldroyd-B fluid were done by Feng, Huang & Joseph (1996) emphasizing wall–particle interactions. Using the same scheme, Huang *et al.* (1997) studied the motion of spherical particles in Couette and Poiseuille flows. A video animation of direct simulation of groups of sedimenting spherical disks by Hu & Joseph (1998) can be seen on our web page; there chains of spheres (disks) line up with gravity and it is natural to ask what holds the chains together and how are the chains stabilized (see figure 2). The existence of aggregated chains of spheres in viscoelastic fluids contrasts with the dispersed arrays of spheres which line up across the stream in Newtonian fluids. What are the underlying mechanisms which lead to such a large difference in the arrangement of spheres sedimenting in Newtonian and viscoelastic fluids?

It is surprising at first sight that turning couples on long bodies determine the stable configurations of suspensions of spherical bodies. A long body is an ellipsoid or a cylinder; a broad body is a flat plate. When such bodies are dropped in Newtonian fluids, they turn and put their longside or broadside perpendicular to the stream. This is an effect of inertia which is usually explained by turning couples at points of stagnation. Milne-Thompson (1968, p. 530) notes that:

> There are many well-known phenomena which are explained in principle by this remark. Thus a ship has to be kept on her course by the helmsman; an elongated airship requires similar attention. A sailing ship will not sail permanently before the wind with the helm lashed, but tends to set itself at right angles to the wind. A body sinking in liquid tends to sink with its longest dimension horizontal.

It is not possible to get long particles to turn broadside in a Stokes flow: bodies in an infinite fluid with fore–aft symmetry do not experience torques. The settling orientation is indeterminate in Stokes flow; however, no matter how small the Reynolds number may be, the body will turn its broadside to the stream; inertia will eventually have its way. When the same long bodies fall slowly in a viscoelastic liquid, they need not put their broadside perpendicular to the stream; they can do the opposite, aligning the long side parallel to the stream.

The flow-induced anisotropy of a sedimenting of fluidized suspension of spheres is determined by the pair interactions between neighbouring spheres. The principle interactions can be described as *drafting*, *kissing* and *tumbling* in Newtonian liquids and as *drafting*, *kissing* and *chaining* in viscoelastic liquids. The drafting and kissing scenarios are surely different, despite appearances. Kissing spheres align with the stream; they are then momentarily long bodies.

The long bodies momentarily formed by kissing spheres are unstable in Newtonian liquids to the same turning couples that turn long bodies broadside-on. Therefore, they tumble. This is a local mechanism which implies that globally the only stable configuration is the one in which the most probable orientation between any pair of neighbouring spheres is across the stream. The consequence of this microstructural property is a flow-induced anisotropy, which leads ubiquitously to lines of spheres across the stream; these are always in evidence in two-dimensional fluidized beds of finite-size spheres. Though they are less stable, planes of spheres in three-dimensional beds can also be found by anyone who cares to look. The long bodies formed by kissing spheres in viscoelastic fluids are stable to turning couples whenever long bodies aligned along the stream are stable.

Joseph & Feng (1996) and Joseph (1996) did analysis of the forces that move particles in slow plane flow of a second-order fluid, a model that applies to our simulations when the Reynolds and Deborah numbers are small. Their analysis can be
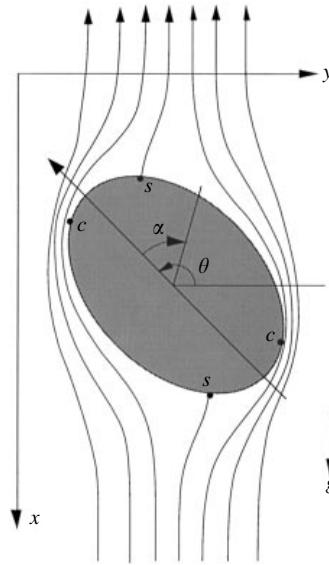
FIGURE 1. Slow flow around an elliptic particle. θ is the tilt angle of the major axis and the horizontal. α is the angle of a typical surface node of the particle. There are two stagnation points s where the shear stress vanishes and two other points c where the streamlines are most crowded. The shear stresses and normal stresses are strongest at c. The nonlinear contribution of the normal stresses in slow flow at each point on the ellipse is given by $-\Psi_1(0)\dot{\gamma}^2$ where $\Psi_1(0) > 0$ is the coefficient of the first normal stress difference and $\dot{\gamma}$ is the shear rate. These normal stresses are compressive and give rise to 'high pressure' at points near where the flow is fast, opposing the high pressure at points s which turn the ellipse broadside-on ($\theta = 180°$) (Joseph & Feng 1996). If the normal stresses at points c dominate at all θ, the major axis of the ellipse will align with gravity ($\theta = 90°$).

used to set the stage for our simulations. They showed that the normal component of the nonlinear elastic part of the normal stress is always compressive and turns long bodies into the stream (see figure 1). Joseph (1996) presented a heuristic argument that normal stresses are amplified by shear thinning at points of high shear. Effects of this amplification by shear thinning are demonstrated in the simulation of Huang *et al.* (1997) and in §12 here.

In all our arguments we suppose that the normal stresses due to viscoelasticity (near c in figure 1) dominate inertial effects (near s in figure 1) which are strongest near stagnation points. Later, we shall argue that these stresses come to dominate when the elasticity number is larger than some critical value.

The sketches shown in figure 2 show how the migrations and orientations of particles are controlled in slow flows by compressive normal stresses $-\Psi_1(0)\dot{\gamma}^2$ which are large where the shear rates are large (indicated by the length of arrows). In general these compressive stresses cause particles to line up, straighten out and aggregate.

In this paper we shall focus our attention on the migration and stable terminal orientation of long bodies settling in viscoelastic fluids. The fluid is assumed to be Oldroyd-B, and computations are done for two cases: Maxwell models in which the ratio of retardation time/relaxation time is zero and when it is 1/8. The Oldroyd-B models have no second normal stress and we shall prove that the normal component of the extra stress vanishes on the boundary of a rigid solid. This means that the effects of inertia and viscoelasticity are to be found only in the reaction pressure evaluated on the body.

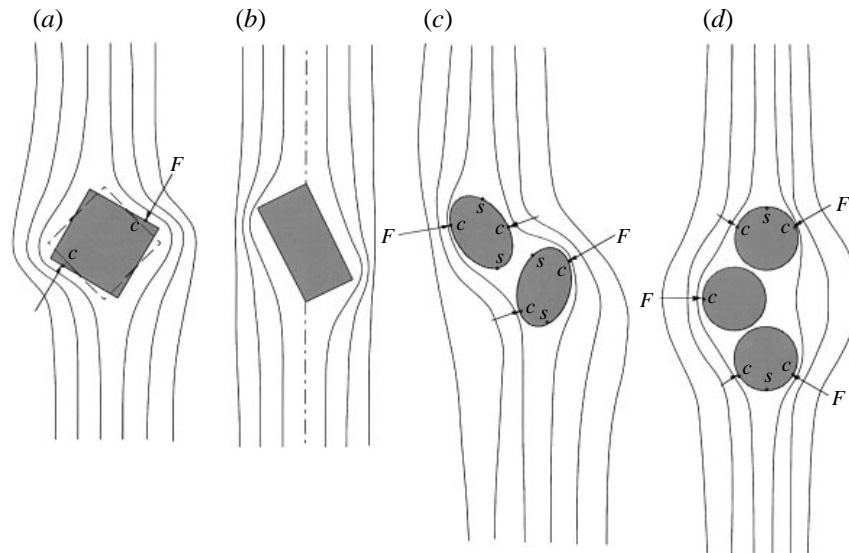Hu, Joseph & Crochet (1992), Feng, Hu & Joseph (1994) and Huang, Feng & Joseph

FIGURE 2. The orientation and migrations of particles in slow flow of a fluid dominated by viscoelasticity can be determined from Stokes flow around that body, with large normal stresses where the shear rates on the body are large, near the places where the streamlines are crowded (see figure 1). (*a*) There are two symmetric orientations with respect to gravity for a falling square (cube): the one with flat faces perpendicular is unstable; the stable orientation is when the line between vertices is parallel to gravity; (*b*) a rectangle or cylinder with flat ends (Joseph & Liu 1993) tends to line up with the longest line in the body parallel to gravity. Falling bodies tilt when the longest line in the body is not an axis of symmetry; this is called shape tilting. (*c*) Falling ellipses tend to straighten out, line up and chain; (*d*) perturbed chains straighten out.

(1994) have shown that an ellipse sedimenting in a Newtonian fluid turns broadside-on but at high Reynolds numbers vortex shedding will make it oscillate.

The orientation of long particles in viscoelastic fluids is broadside-on when inertia dominates and along the stream when viscoelasticity dominates and shape and wall effects are not important. Leal (1975) studied slender cylinders falling slowly in glycerin and in a 0.5% aqueous solution of polyacrylamide (AP-30). He observed that the cylinder rotated into a vertical orientation in the AP-30 solution regardless of the initial orientation. Chiba, Song & Horikawa (1986) studied the motion of a slender body falling in quiescent polymer solutions and in water. They demonstrated that a slender body falling in quiescent polymer solutions and in water. They demonstrated that a slender body falling in Newtonian fluids rotates into a horizontal orientation, whereas in viscoelastic fluids it rotates into a vertical orientation; for less-concentrated solutions it tilts away from vertical and moves sideways as it falls. Liu & Joseph (1993) reported that the orientation of a long body settling in a viscoelastic fluid is determined by a competition between inertia and viscoelasticity. They concluded that visco-elasticity dominates when inertia is small and the particles settle with their broadside parallel to the direction of fall; the same particles settle with their broadside perpendicular to the direction of fall when the inertia is large.

An interpretation of these experiments, analysis and this simulation may be framed in terms of a competition between inertia and normal stresses. The ellipse turns its long side perpendicular to the fall when inertia dominates and parallel to the fall when normal stresses dominate. Tilted orientations of long bodies, neither horizontal or vertical, which are definitely observed in experiments and the numerical simulations

reported here will be interpreted as transient effects arising from walls, as an effect of shear thinning (see §12) or from shape tilting in which the normal stresses tend to line up bodies so that the longest line in the body is turned parallel to the fall; a square body then settles along a line between vertices whereas an ellipse lines its long axis parallel to the flow.

The scenario just described is best framed as a stability hypothesis for two steady states: the ellipse falls with its long axis either vertical or horizontal at a terminal velocity determined by a balance between buoyant weight and drag. A model for this stability hypothesis can be found in Kirchhoff's theory of motion of solid ellipsoids through liquids in potential flow in which the principal axes of the ellipsoid are directions of permanent translation such that if the solid is set moving along one of them without rotation, it will continue to move so. In our two-dimensional problem there are two such directions, one perpendicular and the other parallel to the long side of the ellipse. The solution with long side parallel is unstable to inertia, to couples associated with high pressure at stagnation points as shown in figure 1. We have already noted that viscous effects change many features of the motion of bodies profoundly, but the turning couples from high pressures near stagnation points at the front of a falling ellipse dominate and again turn it across the stream.

Viscoelastic fluids are different from viscous fluids because normal stresses arise both from inertia proportional to the square of the velocity and from elasticity proportional to the square of the shear rate $\dot{\gamma}^2$. The normal stress from inertia is strongest where the flow is slow and the normal stress from viscoelasticity is strongest where the flow is fast (points c in figure 1). The competition between these two normal stresses, one due to inertia and the other to viscoelasticity, could be resolved in angle of tilt in which turning from the two are balanced or they could be unbalanced leading to broadside-on settling when inertia dominates and broadside-along settling when viscoelasticity dominates.

In the case of inviscid and viscous liquids, the steady solution with major axis aligned with gravity or tilted is always unstable; hence only steady solutions with major axis across gravity can be observed. There are no critical stability parameters. But in viscoelastic solutions, long bodies line up with or across the stream, depending on conditions which ought to be described in mathematical terms by critical parameters.

To identify critical parameters, consider the case of an ellipse settling under gravity in an upper-convected Maxwell fluid. The fluid dynamics of such a flow is described by the aspect ratio a/b of the ellipse and two flow parameters:

$$Re = \rho_f Ua/\eta \quad \text{(Reynolds number)},$$

$$De = U\lambda_1/a \quad \text{(Deborah number)},$$

where ρ_f is the density of the fluid, U is the terminal velocity of the ellipse which is determined by a balance buoyant weight and drag, a is the major radius of the ellipse, λ_1 is the relaxation time and η is the viscosity of the fluid. Obviously, these two parameters are independent and any other composition of these two would just be as good; the product

$$(ReDe)^{1/2} = U/(\eta/\lambda_1\rho_f)^{1/2} \overset{\text{def}}{=} M \quad \text{(Mach number)}$$

and the ratio

$$De/Re = \lambda_1\eta/\rho_f a^2 \overset{\text{def}}{=} E \quad \text{(elasticity number)}$$

are even better. The Mach number is the ratio of the terminal velocity to the shear wave

speed $c = (\eta/\lambda_1 \rho_f)^{1/2}$. The elasticity number depends on material parameters and particle size but is independent of flow. It is the ratio of the elastic and inertia forces in the fluid.

Previous works (Liu & Joseph 1993; Joseph & Liu 1993; Joseph 1996) addressed the change in orientation of cylinders of the same size and shape but different weights falling in each of many viscoelastic fluids in terms of the Mach and Reynolds numbers. The light cylinders lined up with the flow, but the heavy cylinders turned broadside-on. This change from vertical to horizontal falling occurs when the stagnation pressures at the front of the falling body are dominated by inertia. For this to happen, the body must fall faster than diffusion $U > \eta/\rho_f a$ (hence $Re > 1$) and faster than shear waves (hence $M > 1$).

The previous results allowed for a range of Mach and Reynolds numbers of order 1 in which the competition of inertia and viscoelasticity could be resolved by a tilt angle in which the terminal orientation of the long side is tilted, neither vertical or horizontal (see Feng *et al.* 1995). In studying the results of the simulation reported here, we have come to believe that the observed tilt is most probably due to wall effects and is either transient or is stabilized by shear thinning. This observation, and a review of the experiments, led Joseph to reformulate the explanations of the observations in terms of the stability of the vertical or horizontal orientation with tilt disallowed. Here we shall promote an explanation of stability framed in terms of the elasticity and Mach numbers. These parameters were advocated as a canonical basis for problems of flow past bodies which change their type, in Joseph (1990, chap. 6).

In the reformulated explanation there are two critical numbers: a critical elasticity and a critical Mach number. Both numbers mark borders in which the balance between inertia and viscoelasticity changes. For elasticity numbers smaller than critical the ellipse falling in an unbounded fluid will turn its long side across the fall, broadside-on, for all speeds, large or small. The critical elasticity number marks the border between effectively Newtonian and effectively viscoelastic behaviour. The ellipse turns broadside-on as in a Newtonian fluid when viscoelastic effects measured by the Deborah number are no larger than a certain measure of inertia involving the Reynolds number; this is expressed precisely by requiring that $E = De/Re$ be smaller than a critical value which we find by simulation. When this ratio is larger than critical, the orientation of the ellipse is reversed, the horizontal orientation is unstable, and the vertical orientation of the long side is stable; it is a dramatic change in stability. Experiments corresponding to changes in the elasticity number were carried out by Chiba *et al.* (1986) who studied the settling of one cylinder in an aqueous solution as a function of concentration, with broadside-on turning for dilute solutions and along-the-stream turning for concentrated solutions. At intermediate concentration tilted cylinders with side drift were observed.

The critical Mach number represents a different physics, corresponding to the experiments of Liu & Joseph (1993) and Joseph & Liu (1993) in which the fluid, and size and shape of particles is fixed and the weight of the particle is varied. Now we focus our attention on effectively viscoelastic fluids in which the elasticity number is greater than critical. In our simulation, described in §7, we may take the critical E as 3 and consider along-the-stream falling with $De/Re = 4$. This means the Deborah number will be four times the Reynolds number no matter what the value of the velocity. The terminal velocity is increased by changing the weight of the particles and when the particle is heavy enough so M passes some number near 1, the particle flips falling broadside-on. In this case the critical M near 1 is a border marking the place at which the fall velocity is larger than the propagation speeds of signals, and is again dominated

by pressures in an effectively potential flow at the front of the body. If this border is at $M = (ReDe)^{1/2} = 1$ and $De = 4Re$, the transition to broadside on turning would occur when $Re = 0.5$.

2. Governing equations

An incompressible fluid is bounded in a two-dimensional region Ω_t with boundary Γ_t formed from fixed walls and contains N rigid particles which can move freely in the fluid. The velocity field $\boldsymbol{u}(\boldsymbol{x}, t)$ and pressure field $p(\boldsymbol{x}, t)$ in the fluid is governed by the equations of motion:

$$\left.\begin{aligned} \boldsymbol{\nabla} \cdot \boldsymbol{u} &= 0, \\ \rho_f \left(\frac{\partial \boldsymbol{u}}{\partial t} + \boldsymbol{u} \cdot \boldsymbol{\nabla} \boldsymbol{u} \right) &= -\boldsymbol{\nabla} p + \boldsymbol{\nabla} \cdot \boldsymbol{T} = \boldsymbol{\nabla} \cdot \boldsymbol{\sigma}, \end{aligned}\right\} \tag{1}$$

where ρ_f is the density of the fluid, $\boldsymbol{\sigma} = -p\mathbf{1} + \boldsymbol{T}$ and $\boldsymbol{T}$ is the extra stress tensor. For an Oldroyd-B fluid, the extra stress tensor is given by the constitutive equation:

$$\boldsymbol{T} + \lambda_1 \overset{\nabla}{\boldsymbol{T}} = \eta(\boldsymbol{A} + \lambda_2 \overset{\nabla}{\boldsymbol{A}}) \tag{2}$$

where $\boldsymbol{A} = (\boldsymbol{\nabla} \boldsymbol{u} + \boldsymbol{\nabla} \boldsymbol{u}^T)$ is the strain-rate tensor; λ_1 and λ_2 are constant relaxation and retardation times; η is the viscosity of the fluid. The fluid reduces to an upper-convected Maxwell model when $\lambda_2 = 0$. The triangle denotes the upper-convected time-derivative:

$$\overset{\nabla}{\boldsymbol{T}} = \frac{\partial \boldsymbol{T}}{\partial t} + \boldsymbol{u} \cdot \boldsymbol{\nabla} \boldsymbol{T} - \boldsymbol{L} \cdot \boldsymbol{T} - \boldsymbol{T} \cdot \boldsymbol{L}^T, \tag{3}$$

where $\boldsymbol{L}_{ij} = \partial u_i / \partial x_j$ is the velocity gradient tensor. Shear thinning can be easily incorporated to the Oldroyd-B model by using the Carreau–Bird viscosity law:

$$\frac{\eta - \eta_\infty}{\eta_0 - \eta_\infty} = [1 + (\lambda_3 \dot{\gamma})^2]^{(n-1)/2}, \tag{4}$$

where $\dot{\gamma}$ is the strain rate defined in terms of the second invariant of $\boldsymbol{A}$ and $0 < n < 1$. The motion of solid particles satisfies the Newton's law:

$$\left.\begin{aligned} \boldsymbol{M} \frac{\mathrm{d} \boldsymbol{U}_p}{\mathrm{d} t} &= \boldsymbol{F}_p + \boldsymbol{G}_p, \\ \frac{\mathrm{d} \boldsymbol{X}_p}{\mathrm{d} t} &= \boldsymbol{U}_p, \end{aligned}\right\} \quad p = 1, 2, \dots, N, \tag{5}$$

where $\boldsymbol{M}$ is the generalized mass matrix of the particle, $\boldsymbol{X}$ and $\boldsymbol{U}$ are the generalized position and velocity vectors of the particle, $\boldsymbol{F}$ is the generalized force vector imposed on the particle by the fluid and $\boldsymbol{G}$ is the body force exerted by external fields such as gravity. The mass matrix $\boldsymbol{M}$ and the vectors can be written explicitly as

$$\boldsymbol{M} = \begin{bmatrix} m & 0 & 0 \\ 0 & m & 0 \\ 0 & 0 & I \end{bmatrix}, \quad \boldsymbol{x} = \begin{bmatrix} X \\ Y \\ \theta \end{bmatrix}, \quad \boldsymbol{U} = \begin{bmatrix} U \\ V \\ \Omega \end{bmatrix},$$
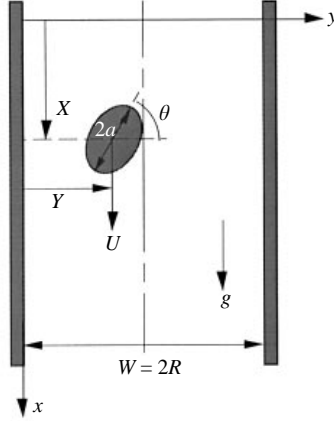
FIGURE 3. Sedimentation of an elliptic particle in a two-dimensional channel. W is the width of the channel. (X, Y) is the position of the centre of the elliptic particle. θ is the orientation of its major axis.

and

$$
\boldsymbol{F} = \begin{bmatrix} F_x \\ F_y \\ F_m \end{bmatrix}, \quad \boldsymbol{G} = (\rho_s - \rho_f) g \pi ab \begin{bmatrix} 1 \\ 0 \\ 0 \end{bmatrix},
$$

where $m = \rho_s \pi ab$ and $I = \frac{1}{4}(a^2 + b^2)\rho_s \pi ab$ are the mass per unit length and the polar moment per unit length of inertia of the elliptic particle. The force and the torque imposed on a solid particle by the fluid is given by

$$
\left.
\begin{aligned}
[F_x, F_y] &= \int_{\Gamma_p} (-p\mathbf{1} + \boldsymbol{T}) \cdot \hat{\boldsymbol{n}} \, d\Gamma, \\
F_m &= \int_{\Gamma_p} (\boldsymbol{x} - \boldsymbol{X}_p) \times (-p\mathbf{1} + \boldsymbol{T}) \cdot \hat{\boldsymbol{n}} \, d\Gamma,
\end{aligned}
\right\}
\tag{6}
$$

where Γ_p is the surface of the particle, $\hat{\boldsymbol{n}}$ is the outward unit normal vector on the surface of particles.

A dimensionless set of governing equations can be obtained from the equations just given by introducing scales: a (semi-major axis) for length, U for velocity, a/U for time, and $\eta U/a$ for stress and pressure. When written in terms of dimensionless variables, using the same symbols for both, we have

$$
\left.
\begin{aligned}
\boldsymbol{\nabla} \cdot \boldsymbol{u} &= 0, \quad Re\left(\frac{\partial \boldsymbol{u}}{\partial t} + \boldsymbol{u} \cdot \boldsymbol{\nabla} \boldsymbol{u}\right) = -\boldsymbol{\nabla} p + \boldsymbol{\nabla} \cdot \boldsymbol{T} = \boldsymbol{\nabla} \cdot \boldsymbol{\sigma}, \quad \boldsymbol{\sigma} = -p\mathbf{1} + \boldsymbol{T}, \\
\boldsymbol{T} + De\, \overset{\nabla}{\boldsymbol{T}} &= \boldsymbol{A} + \frac{\lambda_2}{\lambda_1} De\, \overset{\nabla}{\boldsymbol{A}}, \quad \boldsymbol{F} = \int_{\Gamma} \hat{\boldsymbol{n}} \cdot \boldsymbol{\sigma} \, d\Gamma, \quad F_m = \int_{\Gamma} (\boldsymbol{x} - \boldsymbol{X}) \times \boldsymbol{\sigma} \cdot \hat{\boldsymbol{n}} \, d\Gamma, \\
\pi \frac{a}{b} \frac{\rho_s}{\rho_f} Re \frac{dU}{dt} &= \boldsymbol{F} + \frac{(\rho_s - \rho_f) \pi abg}{\eta U} \boldsymbol{e}_x, \quad \frac{1}{4}\left(1 + \frac{b^2}{a^2}\right) \pi \frac{b}{a} \frac{\rho_s}{\rho_f} Re \frac{d\Omega}{dt} = F_m.
\end{aligned}
\right\}
\tag{7}
$$

The semi-major axis of the dimensionless ellipse is 1 and the semi-minor axis is b/a. The sidewalls are at $x = 0$ and $x = W/a$.

We choose the velocity scale to simplify equation (7):

$$U = (\rho_s - \rho_f)\,\pi abg/\eta. \tag{8}$$

The set of dimensionless parameters which control all possible dynamics of the falling ellipse are

$$\left.\begin{array}{ll} R/a > 1 & \text{blockage ratio,} \\[4pt] a/b \geqslant 1 & \text{aspect ratio,} \\[4pt] \rho_s/\rho_f & \text{density ratio,} \\[4pt] Re = \rho_f Ua/\eta & \text{Reynolds number,} \\[4pt] De = U\lambda_1/a & \text{Deborah number,} \\[4pt] \lambda_2/\lambda_1 \leqslant 1 & \text{retardation/relaxation time ratio.} \end{array}\right\} \tag{9}$$

The viscosity ratio form for shear thinning given by equation (4) is dimensionless.

In our simulation $(\rho_s/\rho_f - 1) \geqslant 0$ is small and ρ_s/ρ_f on the left-hand side of equation (7) could be put to 1 without loss of accuracy. However the difference $(\rho_s - \rho_f)$ is the main parameter used to control velocity.

3. Normal stress at the boundary of a rigid body

Caswell (1967) claims to have proved that all flows become viscometric at a solid surface at rest. Here we consider moving bodies. We find that the turning couples on long bodies and the cross-stream migrations of solid particles are controlled mainly by the pressure. This is no accident; it follows from the fact that the normal component of the extra stress on the boundary of a rigid body vanishes in all incompressible Oldroyd-B fluids. To simplify the demonstration, consider the motion of solid body in two dimensions and pick a generic point on the boundary, calling the direction tangent to the boundary at this point x and the outward normal direction y. Tangential derivatives of velocity vanish along the boundary of a rigid solid even as it moves, and the continuity equation then requires that the normal derivative of normal velocity also vanish. Then, at this boundary point

$$\boldsymbol{L} = \begin{bmatrix} 0 & \dot{\gamma} \\ 0 & 0 \end{bmatrix}, \quad \boldsymbol{A} = \begin{bmatrix} 0 & \dot{\gamma} \\ \dot{\gamma} & 0 \end{bmatrix}, \quad \boldsymbol{T} = \begin{bmatrix} \tau_x & \tau_{xy} \\ \tau_{xy} & \tau_y \end{bmatrix}. \tag{10}$$

The stress is given by

$$\boldsymbol{\sigma} = -p\mathbf{1} + \boldsymbol{T}, \tag{11}$$

where $\boldsymbol{T}$ is the extra stress. For Newtonian fluids $\boldsymbol{T} = \eta\boldsymbol{A}$ and $\tau_x = \tau_y = 0$; hence

$$\sigma_{yy} = \sigma_{xx} = -p \tag{12}$$

at every boundary point. For Oldroyd-B fluids the yy-components of $\boldsymbol{A}$, $\overset{\triangledown}{\boldsymbol{A}}$ and $\boldsymbol{LT}$ vanish and we have

$$\tau_y + \lambda\left(\frac{\partial \tau_y}{\partial t} + U\frac{\partial \tau_y}{\partial x} + V\frac{\partial \tau_y}{\partial y}\right) = 0 \tag{13}$$

or

$$\tau_n + \lambda\left(\frac{\partial \tau_n}{\partial t} + \boldsymbol{U}\cdot\boldsymbol{\nabla}\tau_n\right) = 0, \tag{14}$$

where $\tau_n = \tau_y$ and $U = (U, V)$ is the velocity on the surface of the solid due to rigid body motion. We conclude that $\tau_n = 0$ and

$$\sigma_{nn} = -p \qquad (15)$$

at every point of the boundary of the solid. All the results just given will still hold in three dimensions.

In general, pressure cannot be given *a priori*, but it can be given for potential flows (Joseph & Liao 1994) thorough Bernoulli's equation and in the case of second-order fluids in two dimensions (Tanner 1966) and in three-dimensions when the normal stress coefficients satisfy the condition $\Psi_1 = -2\Psi_2$ (Giesekus 1963). Joseph (1996) and Joseph & Feng (1996) used this result for second-order fluids to obtain an explicit *a priori* expression for σ_{nn} in which the viscoelastic contribution is always compressive and given by $-\frac{1}{2}\Psi_1 \dot{\gamma}^2$ where $\dot{\gamma}$ is the shear rate at the boundary. The normal component of the extra stress $\tau_n = 0$ and $\sigma_{nn} = -p$ at all points of the boundary if and only if the coefficient Ψ_2 of the second normal stress difference vanishes, as it does in Oldroyd-B fluids.

4. Numerical method

Direct simulation of the motion of particles has been carried out by using a two-dimensional generalized Galerkin finite-element method which incorporates both the fluid and particle equations of motion into a single coupled variational equation. An arbitrary Lagrangian–Eulerian (ALE) moving mesh technique was used to compute the motion of the particles. The modified code with the EVSS (elastic-viscous-split-stress) scheme for solving transient equations together with a moving finite-element mesh can be used to simulate the unsteady motion of the viscoelastic fluid and the solid particles directly. In our implementation, the nodes on the particle surface are assumed to move with the particle. The nodes in the interior of the fluid are computed using Laplace's equation, to guarantee a smoothly varying distribution. At each time step, the grid is updated according to the motion of the particles and checked for element degeneration. If unacceptable element distortion is detected, a new finite-element grid is generated and the flow fields are projected from the old grid to the new grid. The fluid is at rest initially and the particles are positioned in the fluid with zero velocity. The particles are then released and the motion of the combined system of viscoelastic fluid and solid particles is computed. In this scheme, the positions of the particles and grid nodes are updated explicitly, while the velocities of the fluid and the solid particles are determined implicitly. In our computations, the elliptic particles at rest initially are heavier than the fluid ($\rho_f = 1.0$ g cm^{-3}) and settle under gravity (figure 3). The inflow boundary of the computational domain is placed $30a$ ahead of the elliptic particle and the outflow boundary is $40a$ behind the particle. We use unstructured triangular elements. A typical mesh used for $R/a = 10$ has 2286 elements and 4688 nodes.

5. Critical Reynolds number for horizontal turning of an ellipse falling in a Newtonian fluid between close walls

Here we shall show that an ellipse which settles in a Newtonian fluid will turn vertical when the Reynolds number is below a critical value, as shown in figure 4. Formerly we thought that inertia would always turn a long particle settling in a Newtonian fluid horizontal at any Reynolds number greater than zero. The only literature we know on
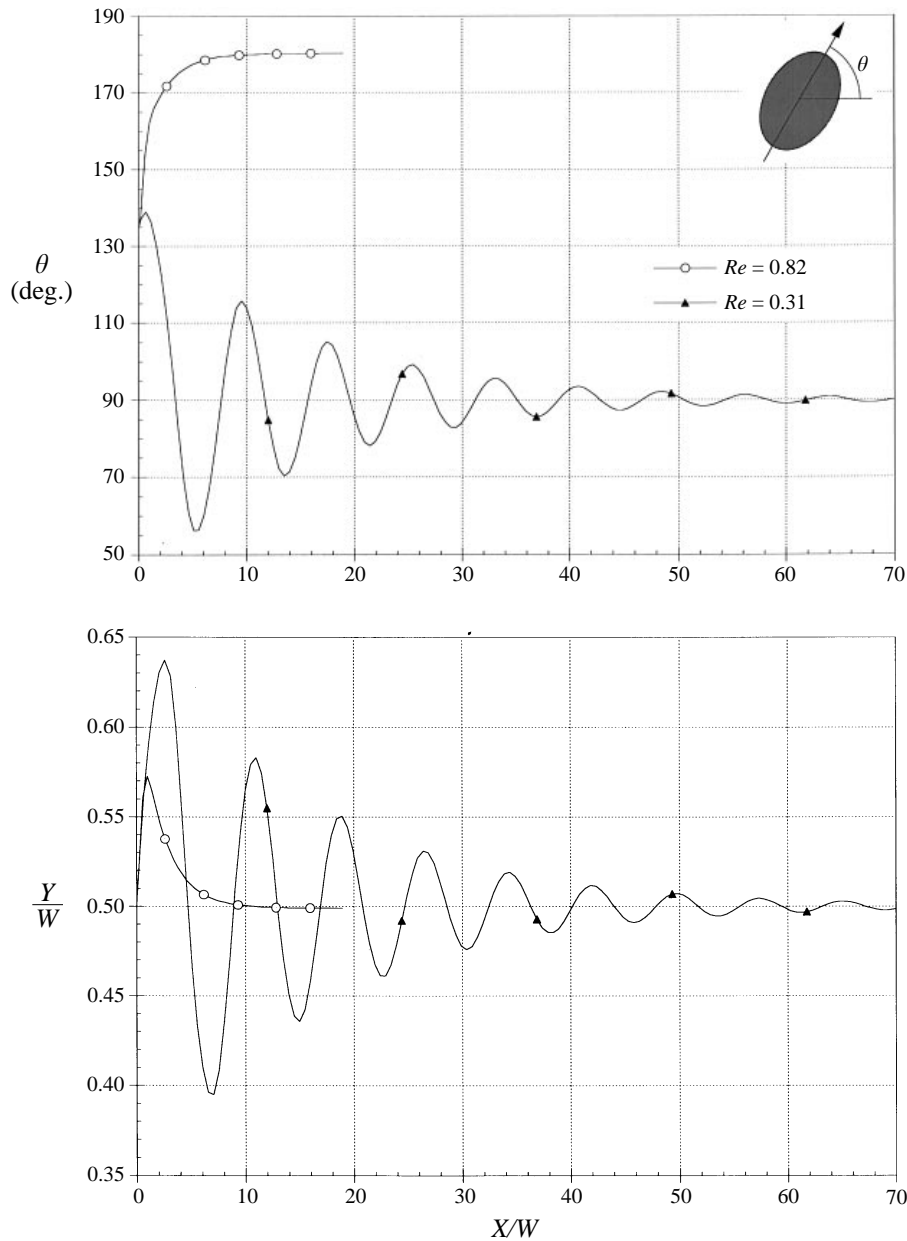
FIGURE 4. Orientation θ and trajectory Y/W of an ellipse ($a/b = 1.5$) settling in a Newtonian fluid ($De = 0$) between close walls ($R/a = 5$). At $Re = 0.31$, the ellipse turns vertical and executes a damped oscillation as it drifts to the channel centre; at $Re = 0.82$, the ellipse turns horizontal as it migrates to the channel centre.

the subject is the numerical study of Huang *et al.* (1994) where the blockage ratio was small ($R/a = 4$) but the Reynolds number is so large ($Re \approx 56$) that only horizontal turning could occur.

Since the numerical result of figure 4 is new and unexpected we did an experiment to see if vertical turning for slow settling between close walls could occur. A cylindrical particle with round ends (see figure 5a) was dropped in a vertical channel. The Newtonian
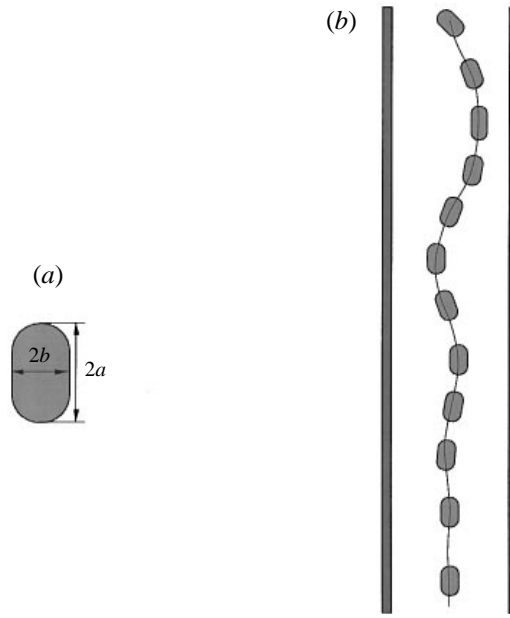
FIGURE 5. (*a*) A plastic long particle with round ends used in the experiment; (*b*) the long particle turns its longside parallel to the stream under the effects of lubrication in a Newtonian fluid when the channel is very narrow and the settling is very slow.

fluid used in the experiment was pure glycerin, with density $\rho_f = 1.26$ g cm^{-3} and viscosity $\mu_f = 13.0$ g cm^{-1} s^{-1}. The solid particle is made of plastic of density $\rho_s = 1.36$ g cm^{-3}. The length of the particle is $2a = 1.32$ cm and the diameter is $2b = 0.635$ cm. The sedimentation channel has a square section with width $W = 2R = 2.2$ cm. The terminal mean sedimenting velocity of the particle is about $V = 0.2$ cm s^{-1}. The controlling dimensionless parameters in the experiment are: the blockage ratio $R/a = 1.7$, the aspect ratio $a/b = 2.1$ and the Reynolds number $Re = \rho_f V a/\mu_f = 0.013$. A sketch of the settling of the solid particle is shown in figure 5(*b*). The particle oscillates before it turns to its equilibrium vertical orientation at the centreline of the channel, as in our numerical computation. When a heavier particle with the same shape and size is dropped, it turns horizontal.

The explanation of vertical turning of an ellipse in a narrow channel is probably found in lubrication forces at low Reynolds number which would tend to produce high pressures in the converging gap between the walls at the top and bottom of the tilted ellipse. These pressures give rise to torques at both ends of the ellipse turning the ellipse vertical. The lubrication pressure is linearly proportional to the velocity of settlement. At higher speeds, stagnation pressures which turn the ellipse horizontal come to dominate.

6. Universal features of equilibrium orientation and positions of an elliptical particle

Many experiments cited in this paper and our simulations are in a range of parameters leading to steady sedimentation so that unsteadiness is transient. After transients decay the ellipse will enter into motion with a permanent character. By an equilibrium we mean steady permanent motion, with a final terminal velocity,
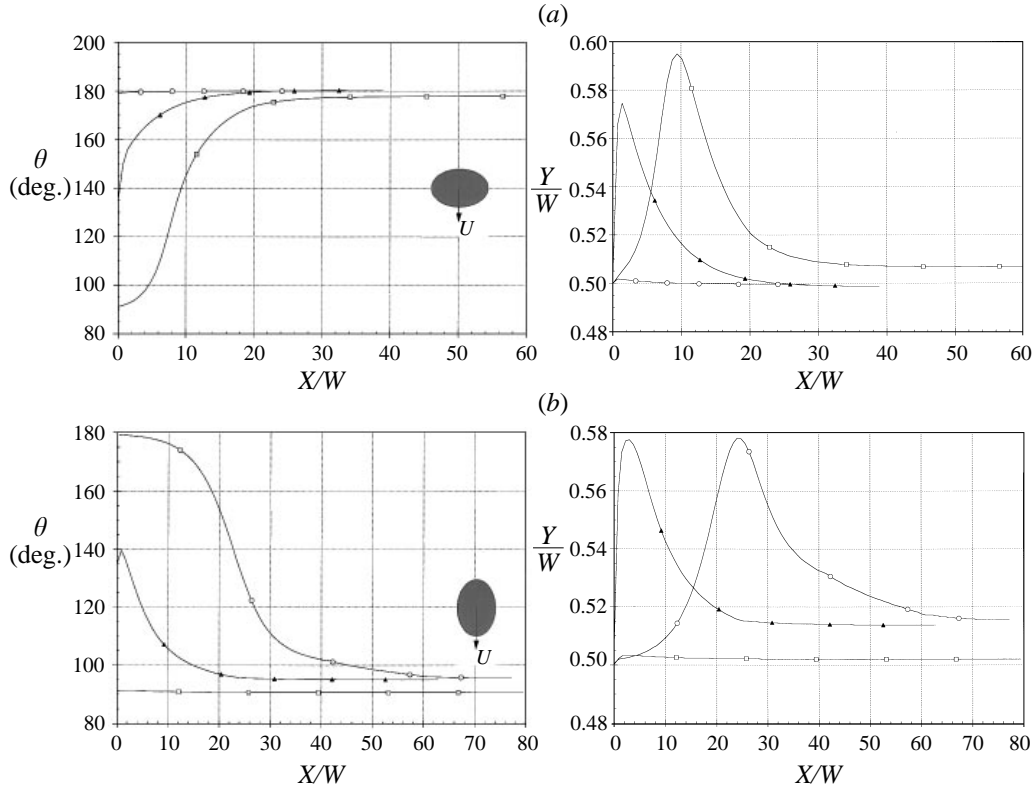
FIGURE 6. The orientation θ and trajectory Y/W of an ellipse of ratio $a/b = 1.5$ falling in a Maxwell fluid in a channel with blockage ratio $R/a = 5$: (a) $E = 0.2$, $Re = 0.82$, $De = 0.16$, $M = 0.37$. The ellipse migrates to the centre and turns horizontal. (b) $E = 0.5$, $Re = 1.00$, $De = 0.50$, $M = 0.71$. The ellipse migrates to the centre and turns vertical.

orientation and no lateral migration. The equilibrium orientation of the ellipse is always perpendicular or parallel to the fall when the final position of the particle centre is at the centre of the channel. This correlation holds for channels of blockage ratio larger than $R/a = 1$ (that we tested), independent of $a/b, \lambda_2/\lambda_1, \rho_s/\rho_f, De$ or Re.

The turning couples on an ellipse are due to inertia and the viscoelastic normal stresses. Since these couples have opposite signs, with magnitudes that vary with the tilt angle, it is possible that tilted zero-torque solutions exist off-centre, stabilized by wall effects. Such solutions can be found but they all appear to be unstable to small perturbations leading again to symmetric orientations at the channel centre.

Assuming now that symmetric orientations at the channel centre are the only stable equilibria, it remains to determine the conditions under which these equilibria are vertical or horizontal. We find critical elasticity, critical Mach and apparently critical blockage numbers to distinguish between stable vertical and horizontal orientations. When the elasticity number is smaller than critical, the ellipse turns broadside-on; above this number stable vertical orientations are found in all cases for which the viscoelastic Mach number is less than a critical Mach number of order unity (see figures 6 and 7). The effect of the blockage ratio is more complicated: we find that the critical elasticity number E is a monotonically increasing function of the blockage ratio R/a with an asymptotic value of E for large R/a and a finite intercept R/a for $E = 0$ (see figure 8).
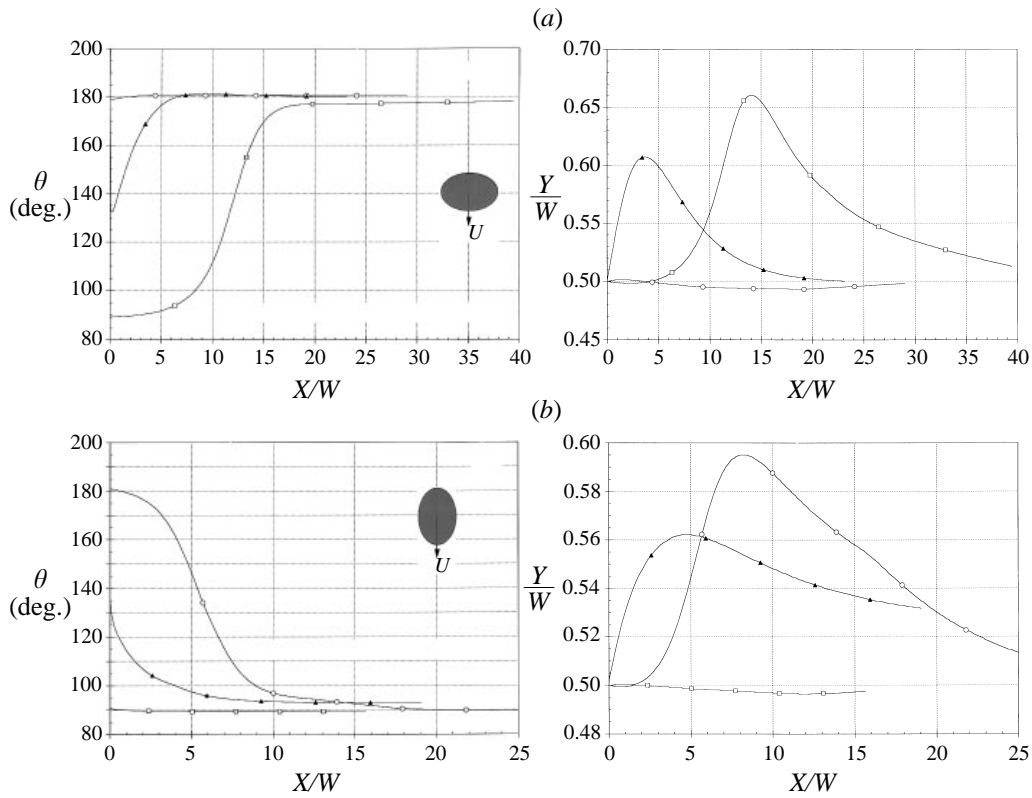
(*a*)

(*b*)

FIGURE 7. The orientation θ and trajectory Y/W of an ellipse of ratio $a/b = 1.5$ falling in a Maxwell fluid in a channel with blockage ratio $R/a = 30$: (*a*) $E = 2.0$, $Re = 0.59$, $De = 1.18$, $M = 0.84$. The ellipse migrates to the centre and turns horizontal. (*b*) $E = 4.0$, $Re = 0.59$, $De = 2.36$, $M = 1.18$. The ellipse migrates to the centre and turns vertical.
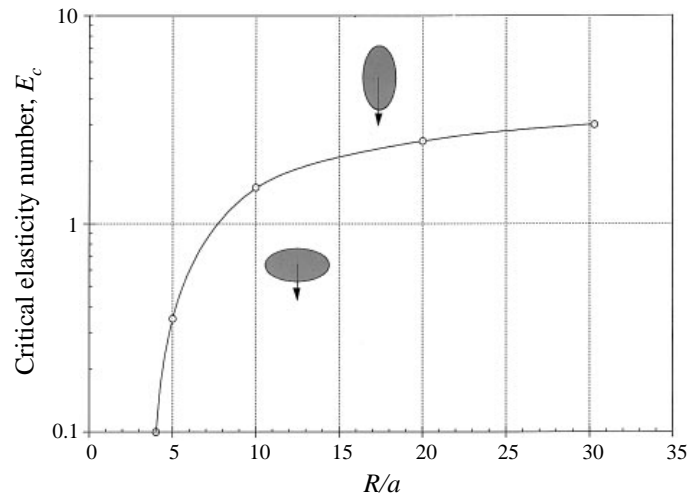

FIGURE 8. Critical elasticity number E_c vs. blockage ratio R/a for ellipses of aspect ratio $a/b = 1.5$ falling in Maxwell fluids. When E is less than critical, inertia dominates as in a Newtonian fluid and the ellipse ultimately falls with its long axis horizontal for all values of the velocity however large, when E is greater than critical the ellipse ultimately falls with its long axis vertical for all Mach numbers less than the critical one.

The critical Mach numbers are associated with the speed of falling particles in the cases in which the elasticity number is greater than critical. In such cases, as we have already mentioned, the ellipse turns vertical apparently at all Mach numbers less than a critical value of order 1; at Mach number greater than this, the ellipse ultimately turns horizontal, just the opposite. Unfortunately, we can play only at the margins of this condition because our simulations fail at high Deborah numbers; the results at this margin are totally consistent with the experiments of Liu & Joseph (1993) and Joseph & Liu (1993).

7. Critical values of elasticity number for Maxwell models ($\lambda_2 = 0$)

Graphs of the evolution of the orientation and trajectory of an ellipse with $a/b = 1.5$ falling in a Maxwell fluid ($\lambda_2 = 0$) in channels with blockage ratios $R/a = 5$ and 30 for values of E above and below the critical value separating vertical from horizontal orientations are shown in figures 6 and 7. We did repeat testing for the critical values and found that the terminal orientation is always vertical or horizontal; tilted orientations are unstable. A summary of these calculations is shown in figure 8. The critical value of E is an increasing function of the blockage ratio R/a with an asymptotic critical value of E slightly larger than 3 for large R/a and $E = 0$ for all positive values of R/a smaller than a critical value slightly less than $R/a = 4$.

8. Critical values of Mach number for Maxwell models ($\lambda_2 = 0$)

The critical Mach number is also a border between vertical and horizontal turning. We fix the elasticity number above critical so that we are dealing with an effectively viscoelastic fluid for which the terminal orientation of a falling ellipse is vertical for all fall velocities smaller than a critical one corresponding to some critical Mach number. To test for the critical Mach number we choose a particle, fluid and sedimentation column fixing E. Then we drop particles of the same size and shape but of different weight. The heavier particles fall faster and at the critical speed the ellipse flips from vertical to horizontal.

Critical speeds were measured in the experiments of Liu & Joseph (1993) and Joseph & Liu (1993) and they correspond to Mach numbers of order 1. $M = 1$ is a critical value for which the vorticity equation in steady flow over a body will change from elliptic to hyperbolic (Joseph 1990); this means that the supercritical flow before a body falling faster than the propagation speed of shear waves is uniform and the forces then are the same pressure forces that turn long bodies broadside-on in Newtonian fluids. Hence, theory and experiments suggest that inertial forces will again dominate effectively viscoelastic fluids with E greater than critical when the viscoelastic Mach number is greater than a critical value of order 1.

Our study of supercritical transitions by numerical methods is at present impeded by the fact that our code does not converge well for high Deborah numbers (De larger than 2 or 3, depending on the Reynolds number). If E_c is the critical elasticity number, then $De = E_c^{1/2} M$ so that our numerical study of supercritical transitions must be restricted to smaller E_c which we get between close walls.

In figure 9 we study the supercritical transition produced by changing the fall speed of a falling ellipse, $a/b = 1.5$, in a Maxwell fluid in a channel of blockage ratio $R/a = 10$ at a value $E = 1.6$ for which the fluid is effectively viscoelastic (see figure 8). The flow with $M = 0.62$ is subcritical; the ellipse migrates to the channel centre and falls finally
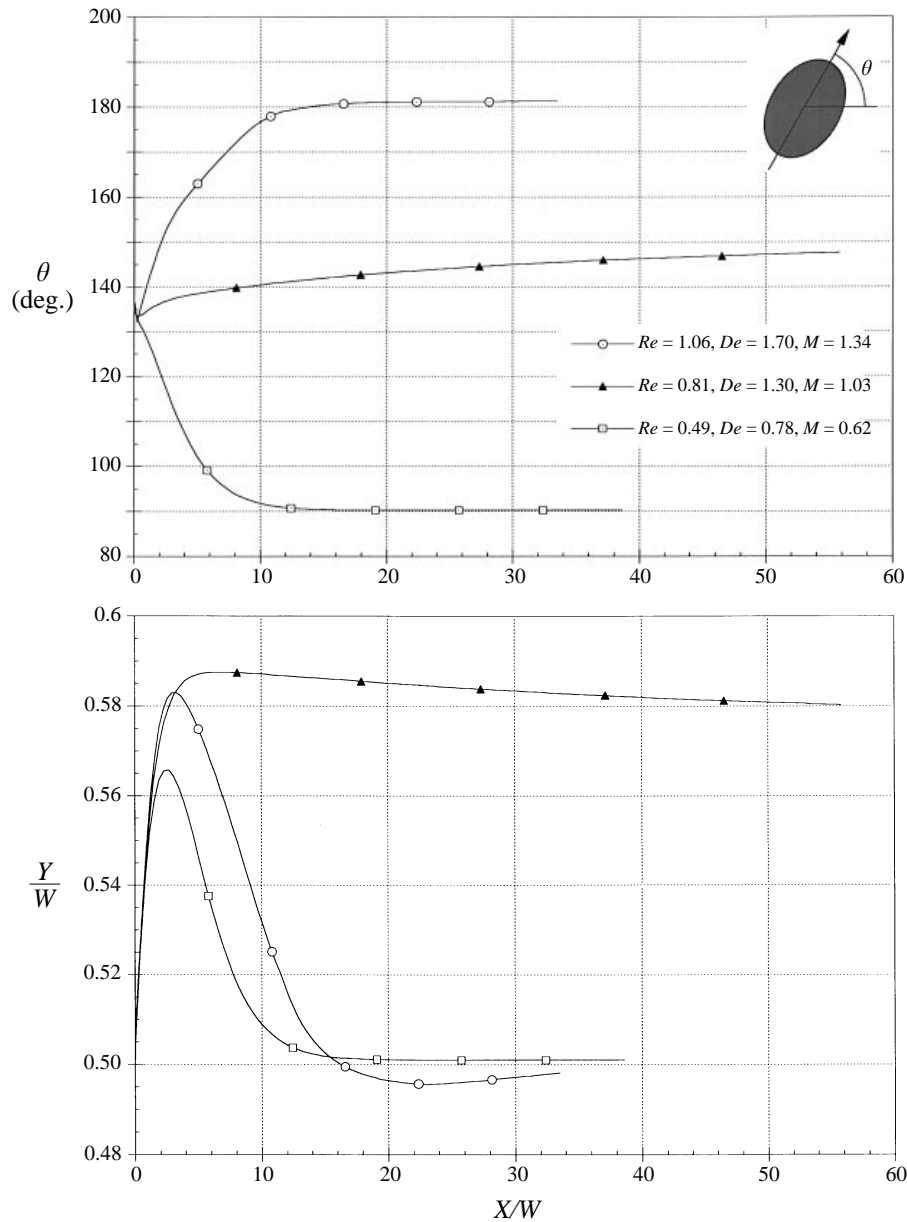
FIGURE 9. The orientation θ and trajectory Y/W of an ellipse of aspect ratio $a/b = 1.5$ falling in a Maxwell fluid in a channel with blockage $R/a = 10$ for $E = De/Re = 1.6$ and different $M:M = 0.62$ ($Re = 0.49$, $De = 0.78$) is subcritical; $M = 1.34$ ($Re = 1.06$, $De = 1.70$) is supercritical; $M = 1.03$ ($Re = 0.81$, $De = 1.30$) is marginally supercritical (see §9).

with its long side vertical. The flow with $M = 1.34$ is supercritical; the ellipse migrates to the channel centre and falls finally with its long side horizontal.

The flow with $M = 1.03$ in figure 9 requires further study; it appears to be a supercritical case in which the evolution toward broadside-on turning is very slow (this slow turning is studied in §9). Assuming now a sharp transition at some critical Mach
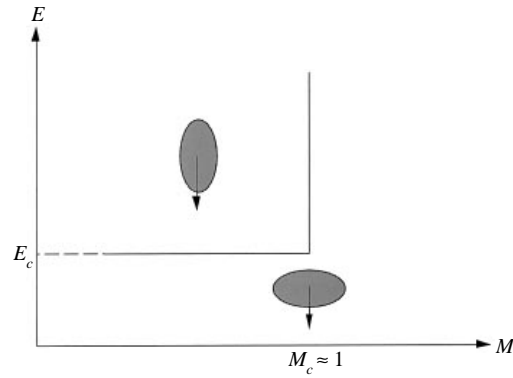
FIGURE 10. Transition diagram for a given blockage ratio $R/a = 10$.
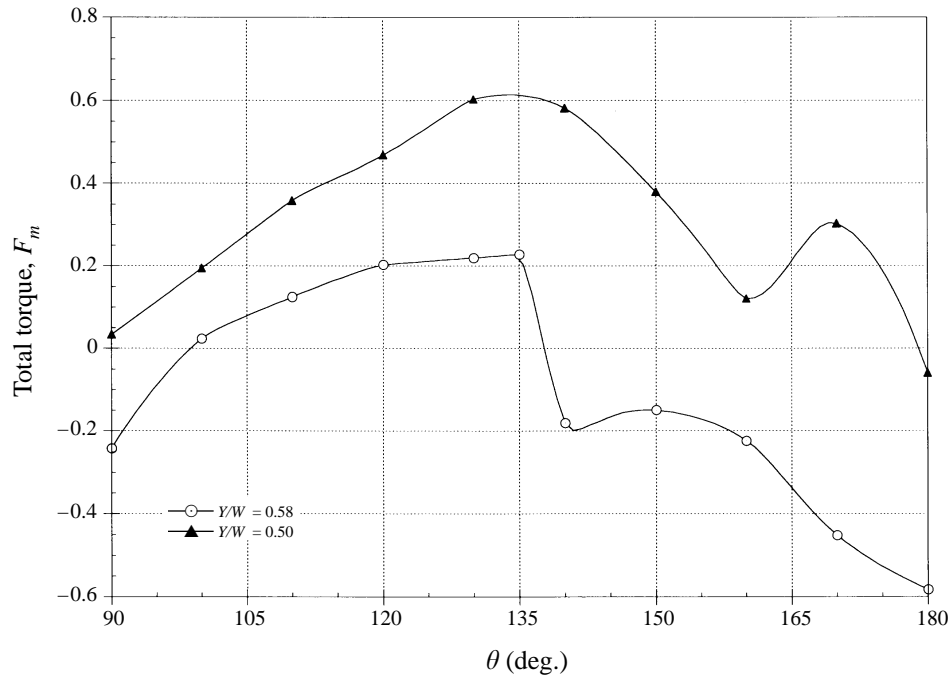
FIGURE 11. Torque on a fixed ellipse of aspect ratio $a/b = 1.5$ in a uniform stream of Maxwell fluid as a function of the orientation of the ellipse for an off-centre ($Y/W = 0.58$) and on-centre position ($Y/W = 0.50$) in a channel with blockage $R/a = 10$ and $E = 1.6$, $M = 1.03$, $Re = 0.81$, $De = 1.30$. There are two zeros for tilted angles in the off-centre case, but the only zero torque positions at the channel centre are for 90° (vertical) and 180° (horizontal).

number near 1 for a given blockage ratio $R/a = 10$, we propose the flow diagram shown in figure 10.

9. Unstable tilted equilibria

The slow evolution toward supercritical broadside-on turning at $M = 1.03$ demonstrated in figure 9 is associated with the existence of an unstable tilted equilibrium. We have already noted in the Introduction that the torques due to inertia and viscoelasticity have different signs so that a zero sum might be generated as the fall
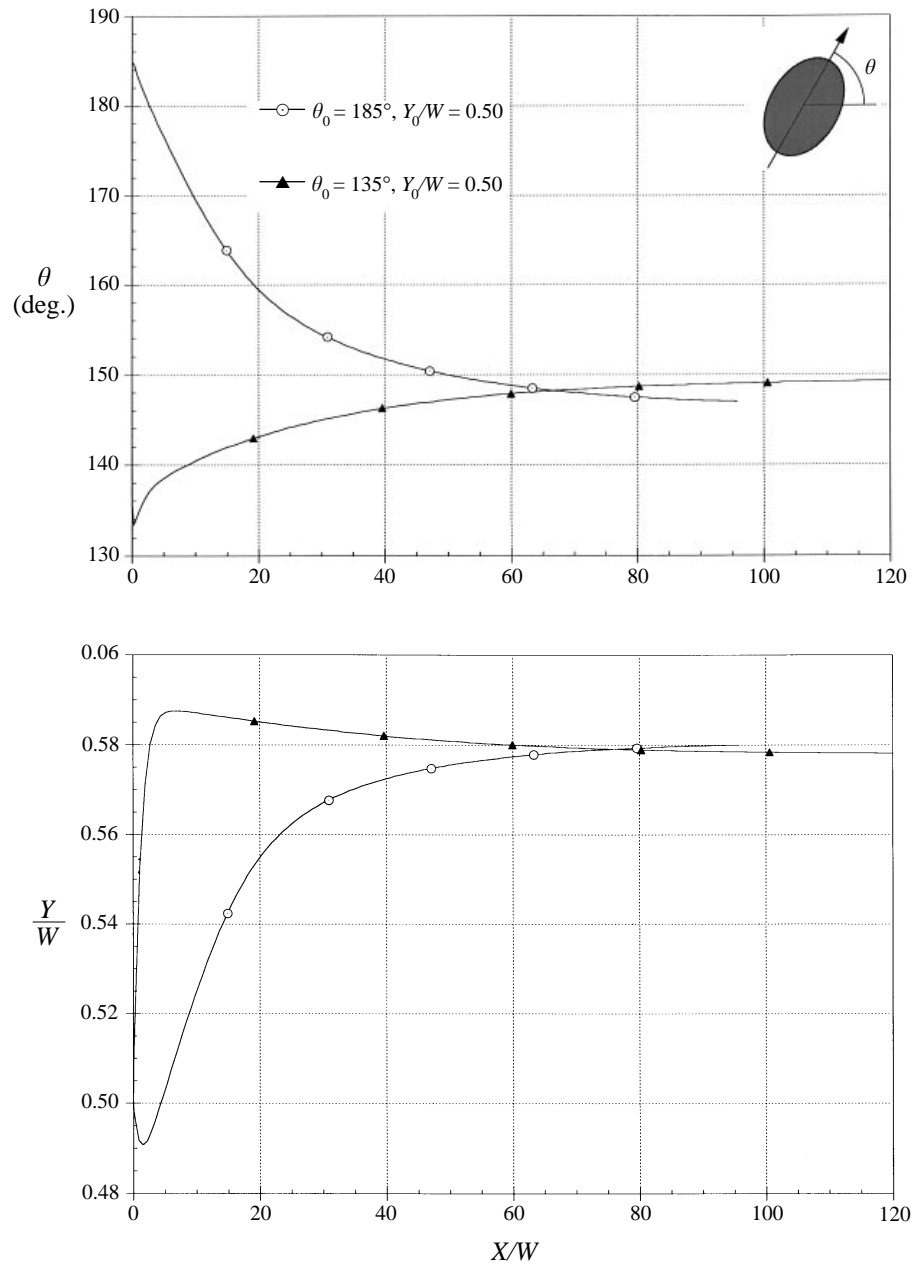
FIGURE 12. The orientation θ and trajectory Y/W of an ellipse of aspect ratio $a/b = 1.5$ falling with two different initial conditions in a Maxwell fluid. $R/a = 10$, $E = 1.6$, $Re = 0.81$, $De = 1.30$ and $M = 1.03$. The ellipse is initially at rest.

velocity is increased through supercritical values for particular angles of tilt; this is why tilted equilibria occur (see Feng *et al.* 1995).

To study tilted equilibria we first carry out a static rather than dynamic calculation. These can be carried out for an ellipse fixed in space immersed in a flow in which a uniform velocity U is prescribed at the inlet of the domain and on both sidewalls. The torque on the ellipse can tell us how it will turn when the constraints are removed.

Now we fix our attention on the case $M = 1.03$ in figure 9. At the end of the calculation the slowly evolving trajectory has reached the value $Y/W = 0.58$, off-centre, with an orientation $\theta = 148°$. Figure 11 gives the value of the total torque for all the orientation angles θ. For $Y/W = 0.58$ we get a zero total torque at two positions, $\theta = 98°$ and $\theta = 140°$. These two positions are candidates for a tilted equilibrium and the one at $\theta = 140°$ could be an attractor for the trajectory belonging to $M = 1.03$.

Figure 12 gives the dynamic simulations of the ellipse of aspect ratio $a/b = 1.5$ falling from two different initial conditions ($\theta = 135°$ and $\theta_o = 185°$ at the centreline) in a Maxwell fluid. The numerical results show that the particle turns to have an equilibrium tilted orientation ($\theta = 148°$) with an off-centre position ($Y/W = 0.58$). However, the results are indecisive since the positions and orientation angles are still changing. In fact, for this type of discrimination our numerical work is indecisive; numerical inaccuracy in the computations is cumulative and long-time results have to be interpreted with care.

Fortunately numerical methods can be used effectively to test the stability of equilibria. Proposing then that $\theta = 148°$ and $Y/W = 0.58$ is a tilted equilibria, we may test for stability by considering the evolution of a small perturbation of this equilibrium. In the present case, we drop an ellipse from rest at $Y/W = 0.58$ with $\theta_0 = 148°$ and see how the evolution evolves. The result is shown in figure 13; the perturbed trajectory migrates to the centreline and the perturbed orientation to broadside-on. Returning now to the static calculation we may verify that the only zero-torque orientations at the channel centre are vertical and horizontal. The broadside-on orientation is stable when $M = 1.03$ and the vertical orientation is unstable. An ellipse which is stable in the vertical position at $E = 1.6$ when the Mach number is less than some critical value near $M = 1$ is unstable when $M = 1.03$ and it turns broadside-on.

10. Effects of the retardation and relaxation time ratio

Now we shall compare the response of an Oldroyd-B fluid with $\lambda_2/\lambda_1 = 1/8$ with an upper-convected Maxwell model $\lambda_2 = 0$; $\eta\lambda_2$ can be interpreted as an effective Newtonian contribution to the total viscosity (Joseph 1990, chap. 18). To get positive normal stresses and other physical properties from an Oldroyd-B fluid, $\lambda_2 \leqslant \lambda_1$. The fluid is Newtonian when $\lambda_2 = \lambda_1$ and is most elastic when $\lambda_2 = 0$. Inertia alone enters when $\lambda_2 = \lambda_1$; hence it ought to be and is true that inertial effects become more important as λ_2/λ_1 is increased from 0 to 1. The effect of increasing the retardation time λ_2 at a fixed value of λ_1 is to make the fluid more Newtonian.

The value $\lambda_2/\lambda_1 = 1/8$ is commonly used in numerical studies for historical reasons only. No one knows how to measure λ_2 and there is no single real fluid for which it can be said that $\lambda_2/\lambda_1 = 1/8$. Many rheologists think that they can put $\eta\lambda_2$ equal to the solvent viscosity in a polymeric solution as was done by Rouse. This doubtful proposition has no foundation in experiments and in any case $\lambda_2/\lambda_1 \neq 1/8$. Joseph (1990) has argued that the effective Newtonian viscosity $\eta\lambda_2$ is a permanent memory relaxed elastic mode.

Some comparisons of Oldroyd-B fluids with $\lambda_2/\lambda_1 = 1/8$ and $\lambda_2 = 0$ are exhibited in figure 14. Figure 14(*a*) shows that $E = 1.2$ is above the critical elasticity number when $\lambda_2 = 0$ and is below the critical E when $\lambda_2/\lambda_1 = 1/8$. The critical E appears to be an increasing function of λ_2/λ_1; there is more broadside turning when the fluid is closer
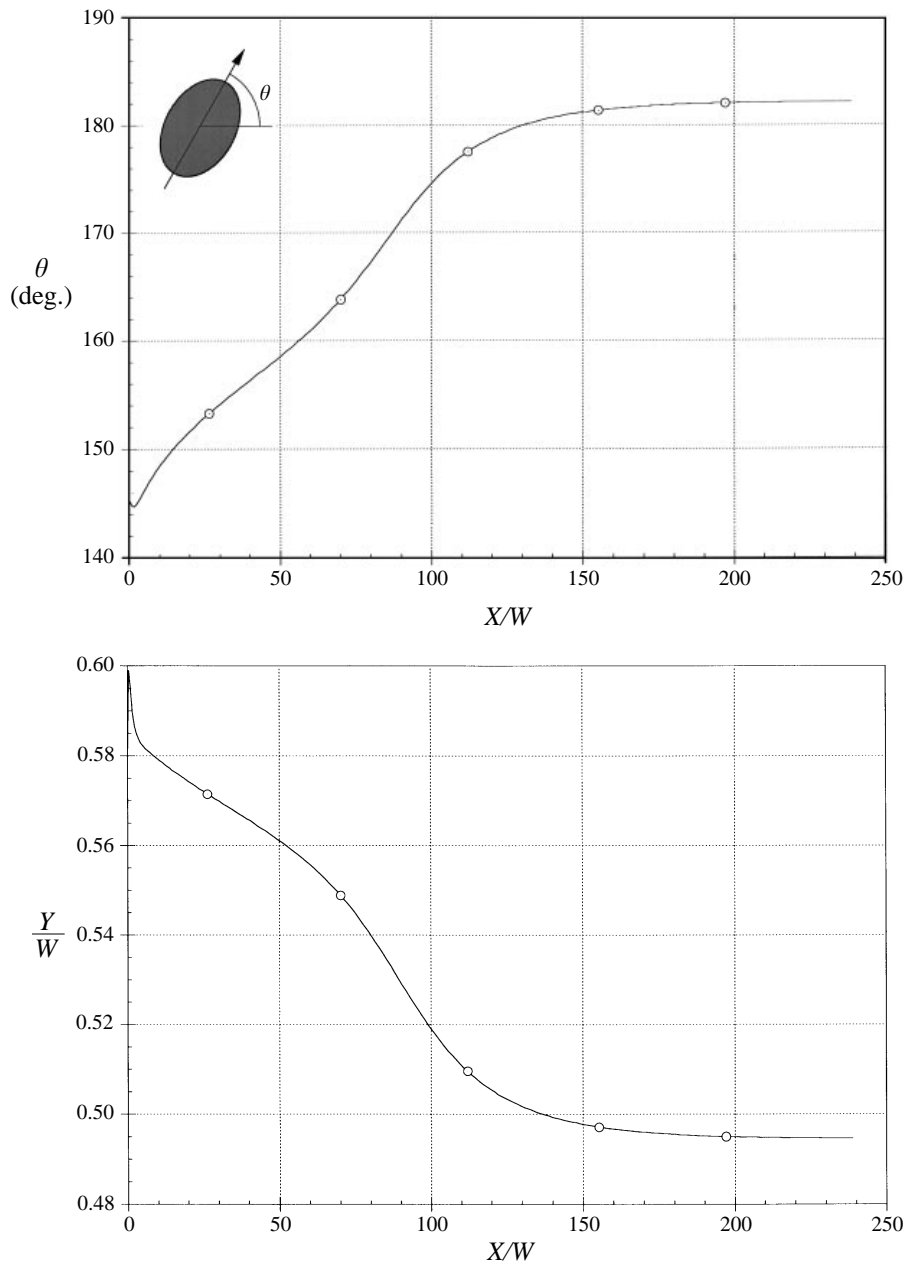
FIGURE 13. Perturbed orientation θ and trajectory Y/W of the ellipse in figure 12 starting from rest near the proposed equilibrium at $\theta = 148°$ and $Y/W = 0.58$. The starting conditions are $\theta = 148°$ and $Y/W = 0.58$. The particle migrates to the centre and turns broadside-on.

to Newtonian; hence $E = 1.2$ is below the critical E when $R/a = 10$ and $\lambda_2/\lambda_1 = 1/8$. Figure 14(*b*) shows that inertia turns a long particle broadside to the stream even in a Maxwell fluid when the effect of elasticity is not large enough ($E = 0.8$). If we eliminate inertia by putting the Reynolds number Re to zero so E goes to infinity, the long particle rotates rapidly into a vertical orientation. Without inertia, the normal stresses produce a torque which rotates the particle straight down.
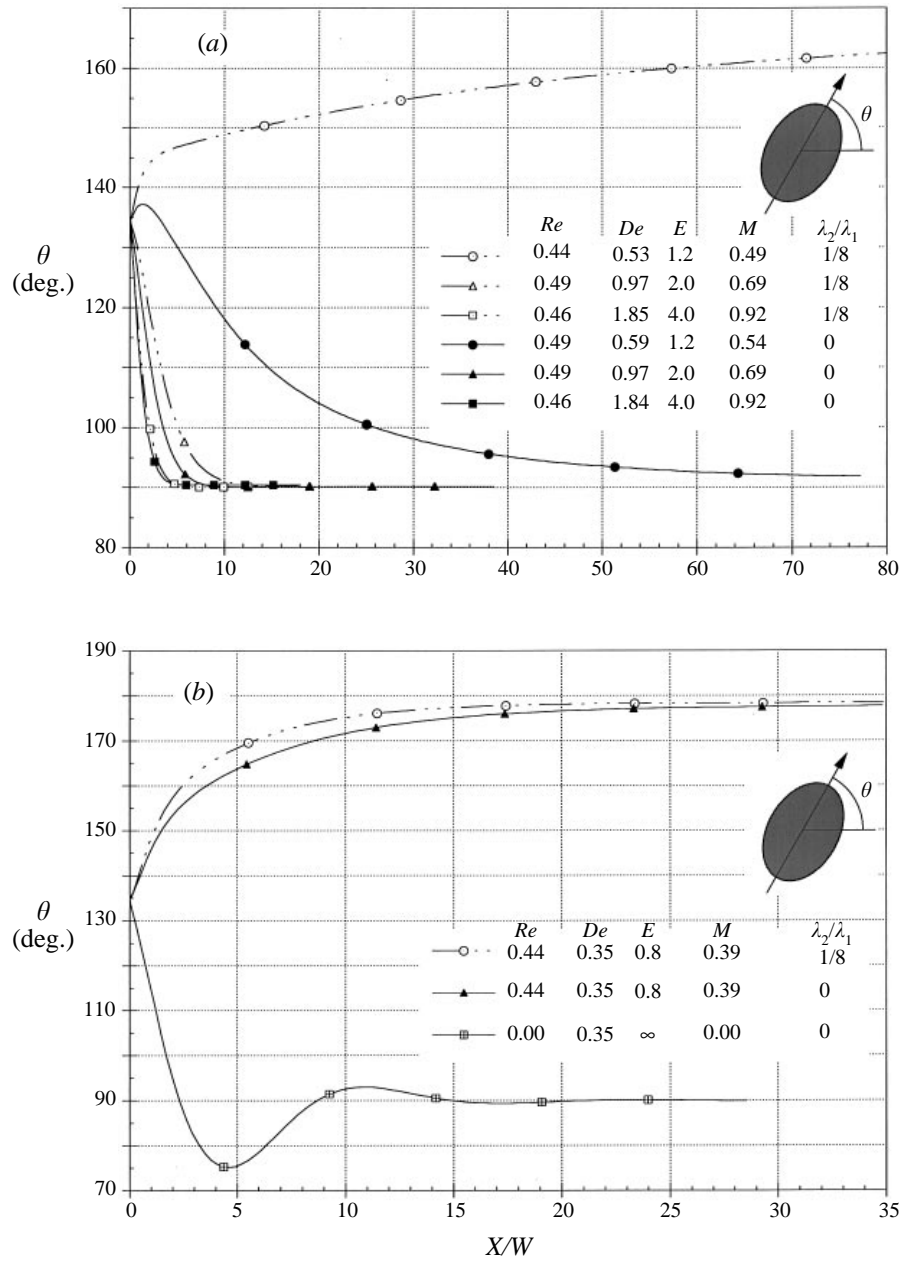
FIGURE 14. Comparison of the orientation of falling ellipses in a Maxwell fluid $\lambda_2 = 0$ to an Oldroyd-B fluid with $\lambda_2/\lambda_1 = 1/8$ ($R/a = 10$, $a/b = 1.5$). Here M is much less than 1 and vertical and horizontal orientations depend on the critical elasticity number, which is higher when $\lambda_2/\lambda_1 = 1/8$. (*a*) The particle settles with its long side vertical when E is above the critical; (*b*) the same particle rotates to horizontal when E is below critical but to vertical when inertia is suppressed ($E = \infty$).

11. Sedimentation of ellipses when $\lambda_2/\lambda_1 = 1/8$

We did a rather large number of computations for this case before taking up the case $\lambda_2/\lambda_1 = 0$. Here we shall summarize the results of this early study.

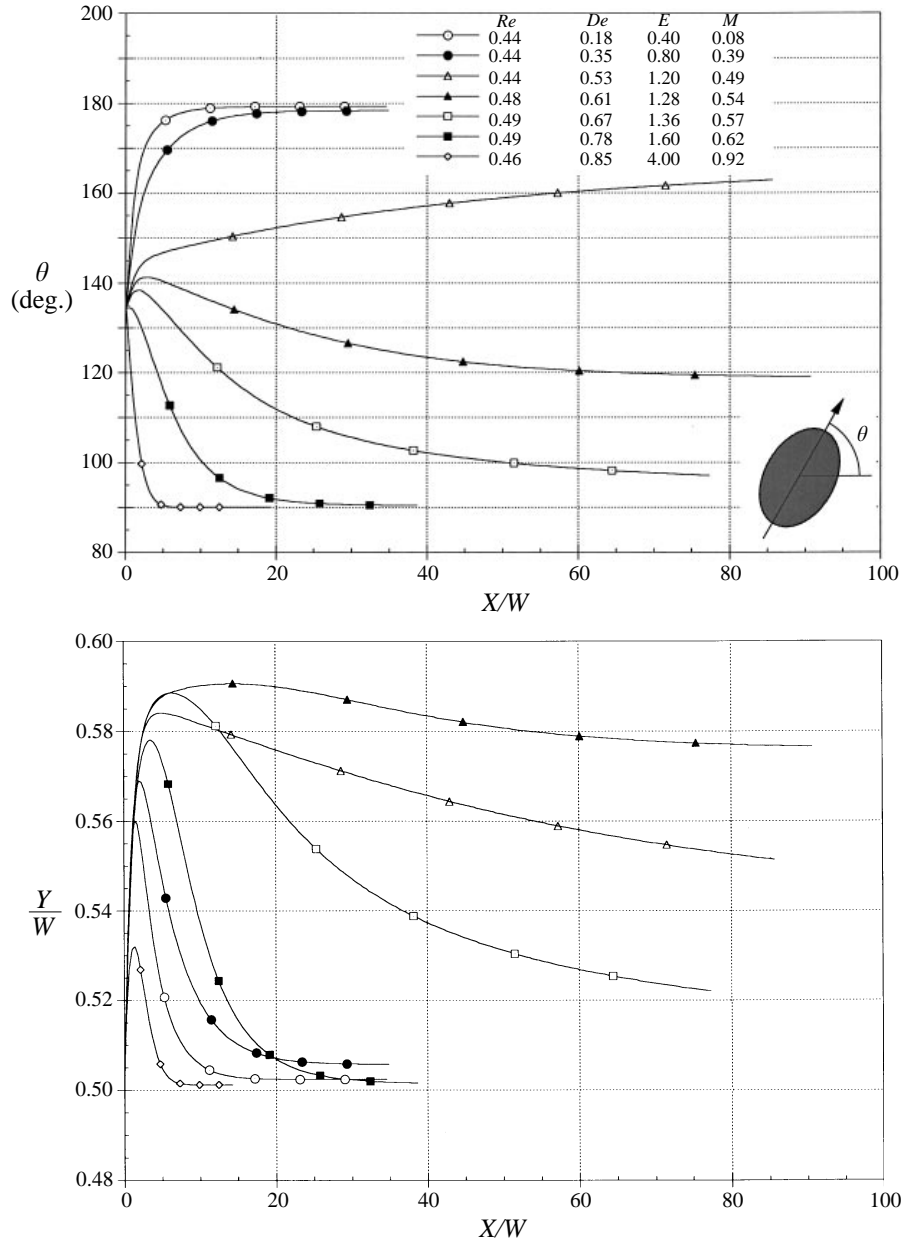| Re	De	E	M
0.44	0.18	0.40	0.08
0.44	0.35	0.80	0.39
0.44	0.53	1.20	0.49
0.48	0.61	1.28	0.54
0.49	0.67	1.36	0.57
0.49	0.78	1.60	0.62
0.46	0.85	4.00	0.92

FIGURE 15. Orientation angle and trajectory of an ellipse as a function of fall distance for different elasticity number corresponding to a fixed Reynolds number ($Re \approx 0.47$) in an Oldroyd-B fluid with $\lambda_2/\lambda_1 = 1/8$ when $R/a = 10$ and $a/b = 1.5$.

11.1. *Critical elasticity number E*

In figure 15 we plotted the orientation and trajectory of subcritical sedimentation of an ellipse of aspect ratio $a/b = 1.5$ in the case specified in the caption of that figure. We kept Re fixed and changed De by changing the relaxation time λ_1. This figure suggests that the critical E for $R/a = 10$ when $\lambda_2/\lambda_1 = 1/8$ is between 1.20 and 1.28. This is a value slightly larger than when $\lambda_2/\lambda_1 = 0$. The elliptic particles eventually turn vertical
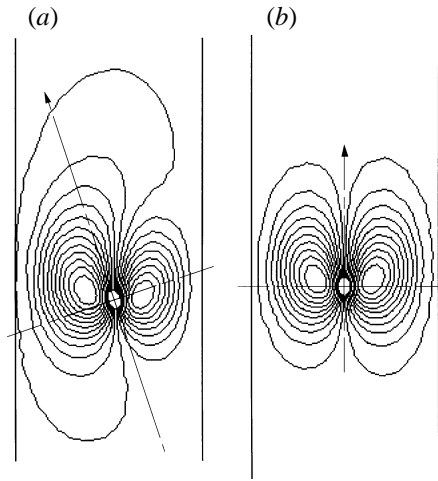
(*a*)　　　　　　(*b*)

FIGURE 16. Streamlines for the flow around an elliptic particle in an Oldroyd-B fluid under conditions specified in figure 15, $R/a = 10$, $a/b = 1.5$, $Re = 0.46$, $De = 1.85$, $E = 4.0$, $M = 0.92$. (*a*) $X/W = 1.375$, $Y/W = 0.532$, $\theta = 108.6°$: the particle is turning clockwise; (*b*) $X/W = 14.32$, $Y/W = 0.501$, $\theta = 90.1°$ the particle has reached an equilibrium in which the major axis is along the stream.
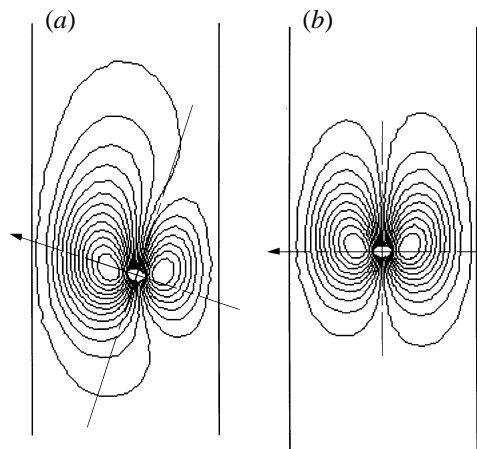
(*a*)　　　　　　(*b*)

FIGURE 17. As figure 16 but $Re = 0.44$, $De = 0.18$, $E = 0.40$, $M = 0.08$. (*a*) $X/W = 1.38$, $Y/W = 0.56$, $\theta = 161.7°$: the particle is turning counter-clockwise; (*b*) $X/W = 34.6$, $Y/W = 0.502$, $\theta = 179.3°$: the particle has reached an equilibrium in which the major axis is across the stream.

or horizontal; this can be shown by stability studies of the type described in §9. The critical M for broadside-on falling is expected to be larger than for the Maxwell model.

11.2. *Streamlines and dynamics of turning ellipses*

Streamlines in a coordinate system on the ellipse under conditions specified in figure 15 are shown in figures 16 and 17. Figure 16 is for a high $De = 1.85$ and $E = 4.0$; figure 16(*a*) shows the particle turning to the vertical equilibrium shown in figure 16(*b*). Clearly the shear rates are large where the flow is fast, producing 'high pressures' there, as shown in figure 1. The normal stresses give rise to a large negative torque which turns the ellipse clockwise, against the high pressure at the front stagnation point.
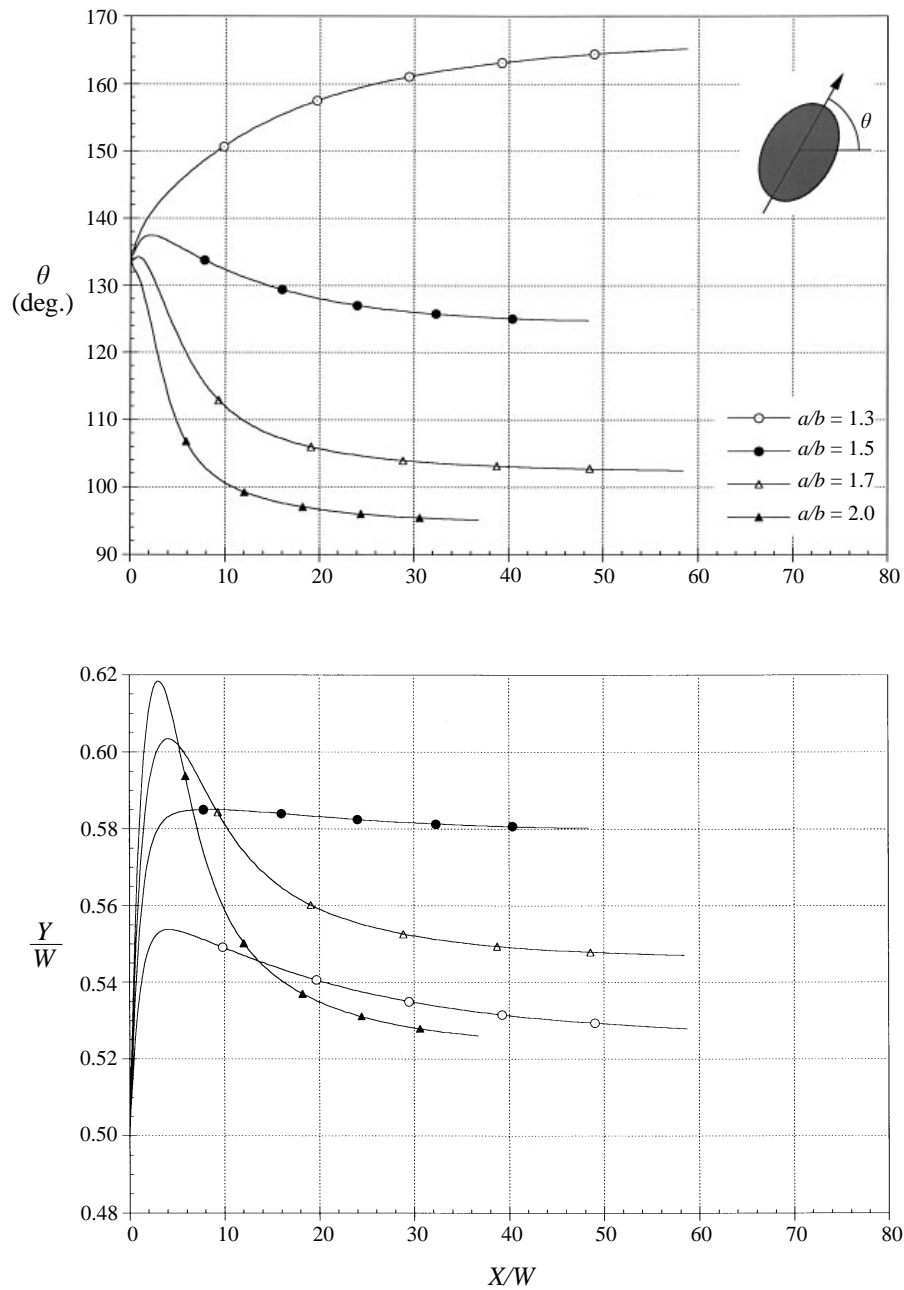
FIGURE 18. Orientation θ and trajectory Y/W of ellipses with different aspect ratios falling in an Oldroyd-B fluid with $\lambda_2/\lambda_1 = 1/8$ ($R/a = 10$, $Re = 0.61$, $De = 0.97$, $E = 1.58$, $M = 0.769$).

Figure 17 is for smaller $De = 0.18$ and $E = 0.40$; the ellipse turns counter-clockwise toward a horizontal equilibrium shown in figure 17(b). The high-shear regions are now located much closer to the two points on the major axis of the ellipse (figure 17a); the compressive normal stresses generate a smaller negative torque on the particle and the front stagnation pressure controls the turning, rotating the particle counter-clockwise.
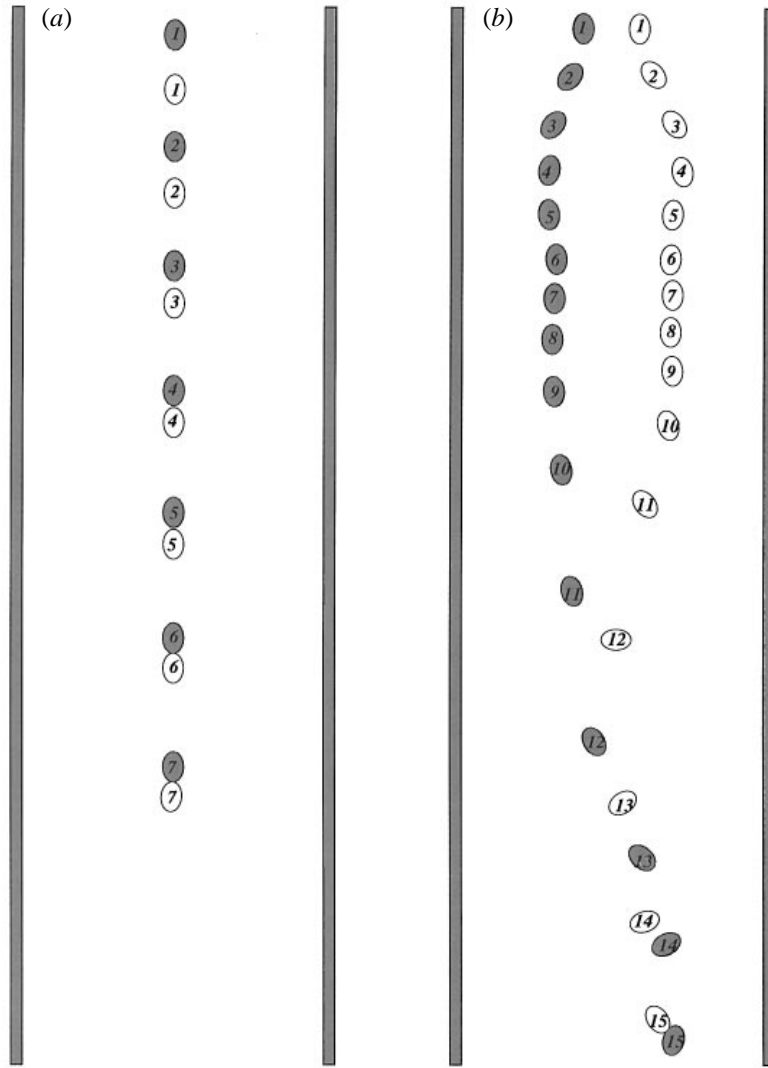
FIGURE 19. The motion of two elliptic particles in an Oldroyd-B fluid ($R/a = 10$, $a/b = 1.5$, $\theta_0 = 90°$). The number on the particles shows the time step. (*a*) Particles are released one on top of the other; (*b*) particles are released side by side.

11.3. *Effects of the particle aspect ratio a/b*

Long thin ellipses turn vertical more readily than short fat ellipses. This suggests that the critical elasticity number is a decreasing function of a/b, viscoelastic effects are amplified. To study effects of viscoelasticity, we change the aspect ratio of the particle a/b, keeping the particle weight constant. The fall velocity changes only slightly under these conditions but particle tilts strongly to the vertical ($\theta = 90°$) as the aspect (or thinness) ratio changes from 1.3 to 2.0, as shown in figure 18.

11.4. *Interaction of two ellipses*

We compute two dynamic simulations of the settling of two elliptic particles with $a/b = 1.5$ in a channel $R/a = 10$ when $\rho_f = 1.0$, $\rho_s/\rho_f = 1.0015$, $\eta = 0.01$, $\lambda_1 = 0.5$ and
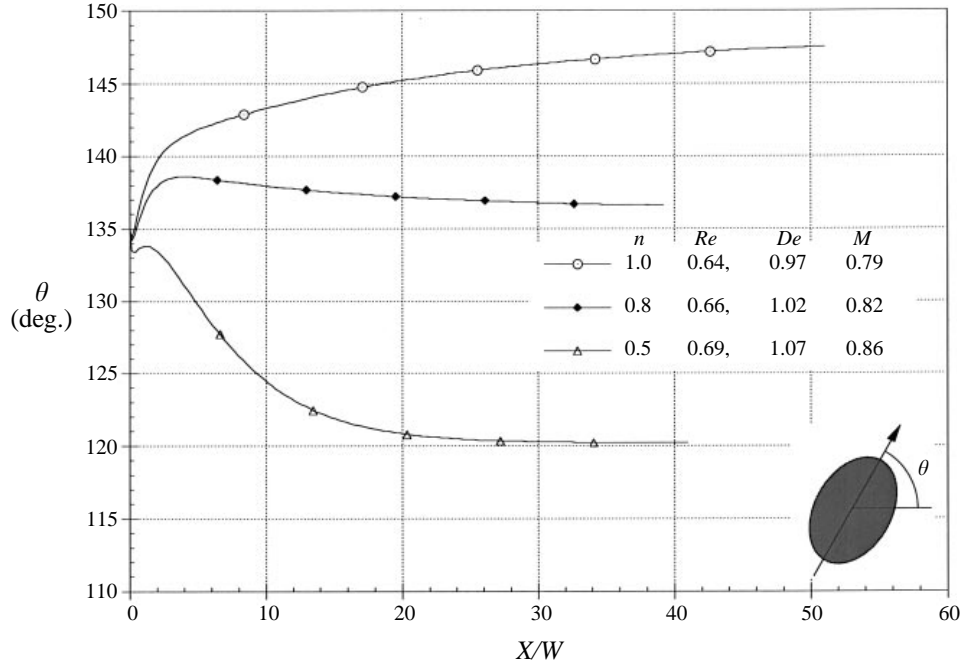
FIGURE 20. The effect of shear thinning on the turning of an elliptic particle in an Oldroyd-B fluid ($R/a = 10$, $a/b = 1.5$, $\lambda_2/\lambda_1 = 1/8$, $E = 1.56$).

$\lambda_2/\lambda_1 = 1/8$. In one simulation, figure 19(a), the particles are dropped one above the other; in the other, figure 19(b), they are dropped side by side. The particles are distinguished by shading and equal numbers are at equal time. Evidently, the particles wish to chain with their major axis vertical. This is consistent with the notion that normal stresses are compressive and of greatest strength where the shear stresses are greatest (see figure 1) as they are at positions of the chain which are out of line, as in figure 19(b). A video animation of the simulation shown in figure 19(b) can be seen on our web page. The simulation in figure 19(b) is terminated at number 15 because of collisions; the smallest distance between particles becomes smaller than the elements in the mesh.

12. Shear thinning

Joseph (1996) has argued, and Huang *et al.* (1997) have shown that the shear thinning amplifies the effects of normal stresses. If the wall shear stress $\tau_w = \eta(\dot{\gamma}_w)\dot{\gamma}_w$ is fixed at the places of high $\dot{\gamma}_w$ (as at points c in figure 1), $\dot{\gamma}_w$ goes up when $\eta(\dot{\gamma}_w)$ decreases. Then, estimating the normal stress by

$$-\Psi_1 \dot{\gamma}_w^2 = -\eta(\dot{\gamma}_w)(\lambda_1 - \lambda_2)\dot{\gamma}_w^2 = -\tau_w \dot{\gamma}_w(\lambda_1 - \lambda_2)$$

in an Oldroyd-B fluid we see that the normal stresses must be larger in the shear-thinning fluid.

Here we study shear thinning by using equation (4) with $\lambda_3/\lambda_1 = 1.0$ and $\eta_\infty/\eta_0 = 0.1$, varying the shear-thinning index n. Other parameters are $R/a = 10$, $a/b = 1.5$, $\lambda_2/\lambda_1 = 1/8$ and $\rho_s/\rho_f = 1.0022$. We fixed the elasticity number near but less than its critical value ($E = 1.56$) so the effects of shear thinning can be seen clearly. For $n =$
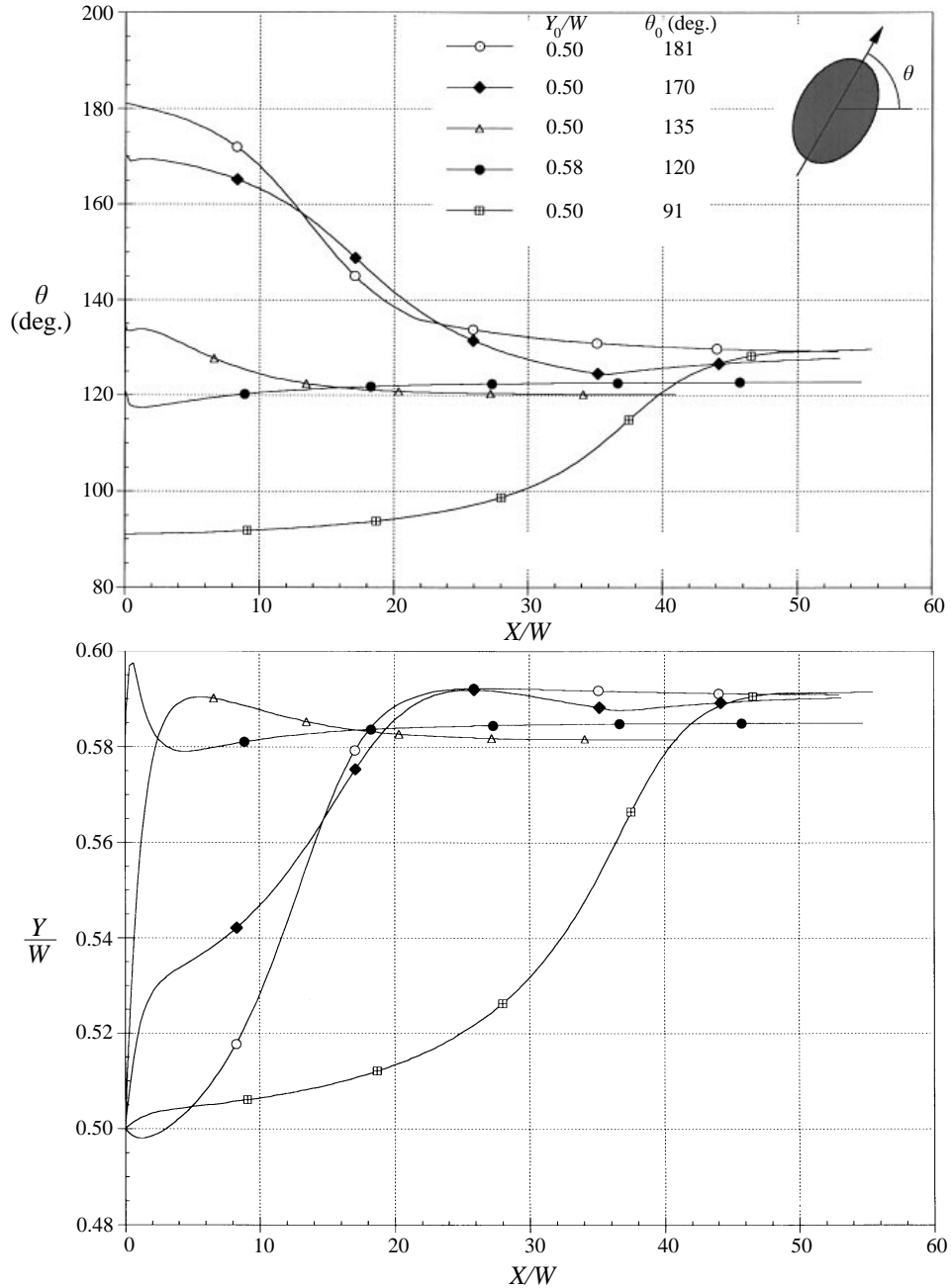
FIGURE 21. Orientation θ and trajectory Y/W of an ellipse released with different initial positions and tilt angles in an Oldroyd-B fluid with shear thinning $n = 0.5$ ($\lambda_2/\lambda_1 = 1/8$, $R/a = 10$, $a/b = 1.5$, $Re = 0.69$, $De = 1.07$, $E = 1.56$, $M = 0.86$). The ellipse migrates to a stable equilibrium off-centre with a certain tilt angle.

1.0, the ellipse migrates to the centre and turns broadside-on. For $n = 0.8$ and $n = 0.5$ the ellipse drifts to an off-centre equilibrium with a certain angle of tilt.

When the fluid does not shear-thin, tilted off-centre equilibria are unstable to small perturbations where the equilibria and evolution of perturbations are computed by

direct simulation (see figure 13). The titled solutions for $n = 0.8$ and $n = 0.5$ shown in figure 20 are stable to these same perturbations, as shown for $n = 0.5$ in figure 21. We are then forced to conclude that tilted equilibrium solutions can be stable if the fluid shear-thins.

We have already mentioned that it is appropriate not to claim too much from simulations whose accuracy for long-time evolution of the orientation and trajectory of a falling ellipse is not perfect. With this reservation, we imagine that the action which produces these off-centre solutions depends on the walls; if a particle is displaced from the centre, the shear, hence the viscosity, is not the same at the left and right side of the particle. This anisotropy of viscosity could be the new feature which opens the possibility of stable tilt. Here, in figure 21, we show that the broadside-on equilibrium which was stable when $n = 1.0$, is unstable when $n = 0.5$.

13. Conclusions

Normal stresses due to inertia turn long bodies across the stream. Normal stresses due to viscoelasticity turn long bodies along the stream. The orientation is determined by a competition between normal stresses due to inertia and viscoelasticity.

The normal stresses associated with the extra stresses on moving rigid bodies vanish. The normal stresses on rigid bodies due to all causes are contained in the pressure alone. It may be true that the normal stresses on rigid bodies associated with extra stresses vanish in all fluids in which the second normal stress vanishes.

An ellipse falling in an Oldroyd-B fluid between plane walls can evolve into a time-dependent motion or steady falling. Stable steady flows are at the channel centre and are not tilted.

A critical value of the elasticity number can be determined. For values of the elasticity number below critical, the fluid is effectively Newtonian in the sense that the final orientation is broadside-on for all values of the fall velocity.

For values of the elasticity number larger than critical, the ellipse finally settles with its long axis vertical provided that it does not fall too fast.

When the elasticity number is greater than critical, a critical Mach number can be found. For Maxwell models the critical Mach number is close to 1. When the fall velocity is such that the Mach number is larger than critical, the ellipse falling vertically will flip to horizontal.

A non-zero critical elasticity number can be determined only for channels whose walls are not too close. There is a critical blockage ratio (ratio of channel width to particle diameter) below which no critical elasticity number can be determined. The critical elasticity number is an increasing function of the blockage ratio R/a tending to some finite value as the distance between channel walls is increased.

When the channel walls are close together (small blockage ratio), an ellipse settling slowly in a Newtonian fluid will settle with its long axis vertical. This numerical result was verified in an experiment. At faster speeds the ellipse settling in a Newtonian turns broadside-on.

Tilted equilibria can also be generated by shear thinning which generates variable flow-induced viscosity which is not symmetric with respect to the falling particle.

The effects of elasticity are enhanced in thinner ellipses. The critical elasticity number is a decreasing function of the aspect ratio a/b.

The effect of increasing the retardation/relaxation time ratio λ_2/λ_1 is to make the fluid more Newtonian; it is Newtonian when this ratio is 1.

There is a tendency for particles which fall slowly in viscoelastic fluids above the

critical elasticity number to line up with the longest line in the body parallel with gravity; for a square body or cube this long line is from vertex to vertex. This effect, which causes cylinders with flat ends, or particles whose longest diameter is not centrally located, to tilt is well documented in the experiments of Liu & Joseph (1993), of Joseph & Liu (1993) and is explained theoretically by Joseph (1996). The sedimentations for these kinds of particles have not yet been computed by direct numerical simulation.

REFERENCES

CASWELL, B. 1967 Kinematics and stress on a surface of rest. *Arch. Rat. Mech. Anal.* **26**, 385–399.

CHIBA, K., SONG, K. & HORIKAWA, A. 1986 Motion of a slender body in quiescent polymer solutions. *Rheol. Acta* **25**, 380–388.

FENG, J., HU, H. H. & JOSEPH, D. D. 1994 Direct simulation of initial value problems for the motion of solid bodies in a Newtonian fluid. Part 1. Sedimentation. *J. Fluid Mech.* **261**, 95–134.

FENG, J., HUANG, P. Y. & JOSEPH, D. D. 1996 Dynamic simulation of sedimentation of solid particles in an Oldroyd-B fluid. *J. Non-Newtonian Fluid Mech.* **63**, 63–88.

FENG, J., JOSEPH, D. D., GLOWINSKI, R. & PAN, T. W. 1995 A three-dimensional computation of the force and torque on an ellipsoid settling slowly through a viscoelastic fluid. *J. Fluid Mech.* **283**, 1–16.

GIESEKUS, H. 1963 Die Simultane Translations- und Rotationsbewegung einer Kugel in einer elastoviskosen Flüssigkeit. *Rheol. Acta* **3**, 59–71.

HU, H. H. 1996 Direct simulation of flows of solid-liquid mixtures. *Intl J. Multiphase Flow* **22**, 335–352.

HU, H. H. & JOSEPH, D. D. 1998 Simulation of particle motion in viscoelastic fluids. In preparation.

HU, H. H., JOSEPH, D. D. & CROCHET, M. J. 1992 Direct simulation of fluid particle motions. *Theor. Comput. Fluid Dyn.* **3**, 285–306.

HUANG, P. Y., FENG, J., HU, H. H. & JOSEPH, D. D. 1997 Direct simulation of the motion of solid particles in Couette and Poiseuille flows of viscoelastic fluids. *J. Fluid Mech.* **343**, 73–94.

HUANG, P. Y., FENG, J. & JOSEPH, D. D. 1994 The turning couples on an elliptic particle settling in a vertical channel. *J. Fluid Mech.* **271**, 1–16.

JOSEPH, D. D. 1990 *Fluid Dynamics of Viscoelastic Liquids*. Springer.

JOSEPH, D. D. 1996 Flow induced microstructure in Newtonian and viscoelastic fluids. In *Proc. 5th World Congress of Chem. Engng, Particle Technology Track, San Diego. July 14–18. AIChE* **6**, 3–16.

JOSEPH, D. D. & FENG, J. 1996 A note on the forces that move particles in a second-order fluid. *J. Non-Newtonian Fluid Mech.* **64**, 299–302.

JOSEPH, D. D. & LIAO, T. Y. 1994 Potential flows of viscous and viscoelastic fluids. *J. Fluid Mech.* **265**, 1–23.

JOSEPH, D. D. & LIU, Y. J. 1993 Orientation of long bodies falling in a viscoelastic liquid. *J. Rheol.* **37**, 961–983.

LEAL, L. G. 1975 The slow motion of a slender rod-like particles in a second-order fluid. *J. Fluid Mech.* **69**, 305–337.

LIU, Y. J. & JOSEPH, D. D. 1993 Sedimentation of particles in polymer solutions. *J. Fluid Mech.* **255**, 565–595.

MILNE-THOMSON, L. M. 1968 *Theoretical Hydrodynamics*. Macmillan.

TANNER, R. I. 1966 Plane creeping flows of incompressible second-order fluids. *Phys. Fluids* **9**, 1246–1247.